



Synthesis and thermoluminescence study of Dy³⁺ doped ZnAl₂O₄ phosphor for high-dose dosimetry application

Ajay D. Vartha^{1,2} · Pratik R. Patankar¹ · P. D. Sahare³ · Lucky Sharma³ · Avinash R. Kachere¹ · Prashant M. Kakade¹ · Bhuli Bai³ · Sanjay D. Dhole⁴ · Nandkumar T. Mandlik¹

Received: 31 August 2023 / Accepted: 21 May 2024 / Published online: 2 July 2024
© Akadémiai Kiadó, Budapest, Hungary 2024

Abstract

ZnAl₂O₄:Dy³⁺ sub-micron phosphor material was synthesized by co-precipitation method. Different characterization techniques, including XRD, FESEM, FTIR, TG–DTA, UV–visible spectroscopy, Photoluminescence (PL) and Thermoluminescence (TL) were used to investigate different properties of the material. Effects of doping concentration and heat treatments on the TL properties were investigated. It was observed that the ZnAl₂O₄:Dy³⁺ (0.2 M%) phosphor material exhibited its maximum TL intensity when annealed at 1600 °C. Kinetic parameters were determined by different methods, such as, Computerized Glow Curve Deconvolution (CGCD) method, Initial Rise (IR) method and Various Heating Rate (VHR) method. The phosphor showed excellent TL properties like good reusability, wide and sublinear dose response which makes it a suitable candidate for high-dose dosimetry application.

Keywords Dy³⁺-doped zinc aluminate · Co-precipitation method · Thermoluminescence (TL) · Photoluminescence (PL) · TLD phosphor material

Introduction

It has been more than 400 years since Robert Boyle has accidentally discovered Thermoluminescence (TL) in a diamond. Since then, there has been momentous development in the investigation of the TL properties of the phosphors for various applications including radiation dosimetry. TL is a phenomenon in which energy stored in an irradiated material in the form of defects and it is released when subjected to the

heat. After heating the pre-irradiated phosphor, the trapped electrons are freed from trapping centers and recombine with holes called luminescence centers (LCs) by releasing energy of recombination in the form of photons which are measured using photodetectors. The number of traps/LCs are generally proportional to the absorbed doses. Thus, by using a simple technique, such as TL, the doses of high energy radiations could be estimated. Recently, extensive research has been carried out on the rare earth-activated phosphor materials for their effective application in the field of radiation dosimetry [1].

The TL dosimetry technique, along with other applications, is widely utilized in the field of ‘dosimetry for irradiation of food’ where high doses of ionizing radiations are used. The useful range of high dose dosimetry is found to be in the range of 10 Gy to a few kGy [2]. There are many TLD phosphor that are commercially available, including LiF:Mg,Ti (TLD-100), CaF₂:Dy (TLD-200), LiF:Mg,Cu,P (TLD-700H), Al₂O₃:C (TLD-500), and CaSO₄:Dy (TLD-900) for their applications in radiation therapy, personal dosimetry, and environmental monitoring, etc. [3, 4]. The majority of these phosphors could be utilized for measurement of high doses because they saturate early (~ 100 Gy) [5]. There is also a problem of radiation hardening and

✉ P. D. Sahare
pdsahare@yahoo.co.in

✉ Nandkumar T. Mandlik
nandkumar.mandlik@fergusson.edu

¹ Department of Physics, Fergusson College (Autonomous), Savitribai Phule Pune University, Pune, Maharashtra 411004, India

² Department of Physics, Loknete Ramsheth Thakur, Arts, Science and Commerce College (Mumbai University), Makhada, Maharashtra 401604, India

³ Department of Physics and Astrophysics, University of Delhi, Delhi 110007, India

⁴ Department of Physics, Savitribai Phule Pune University, Pune, Maharashtra 411007, India

reusability at very high doses. Recently, Sahare et al. [6–22] have shown that TLD nanophosphors have very wide dose ranges (10^{-3} to 10^5 Gy) and especially used for estimation of high doses (as high as 10^5 Gy) of ionizing radiations like gamma rays. Moreover, they are more radiation resistant too. Recent papers on the TL also show that some microcrystalline TLD phosphor materials could also be used for estimation of high doses of such radiations [23–25] and efforts are still being made to discover such phosphors (aluminates, sulphates, borates, etc.) which would detect high dose without undergoing structural damages by preparing them in various ways, subjecting them to heat treatments in different reducing/oxidizing atmospheres and/or doping/codoping them with different impurities.

Researchers working worldwide have discovered remarkable properties of zinc aluminate (ZnAl_2O_4) phosphor, such as, wide band gap ($E_g \approx 3.8$ eV), high thermal stability, better diffusion and excellent ductility, etc. It has been widely used for many applications, such as, catalysis, sensor and radiation dosimetry [26–30]. Rare earth doped zinc aluminate compounds have received a significant attention due to its noteworthy thermoluminescent properties, such as, wide and linear dose response, excellent reusability, low fading, etc. However, it is not easy to prepare the material in a single phase as traces of ZnO and Al_2O_3 unreacted phases could also be found in the material, if it is not sintered properly at higher temperatures (as high as 1600 °C and above). This may affect dosimetry properties, such as glow curve structure, sensitivity, dose response etc. This has not been explored till today for dosimetry applications. Synthesis of zinc aluminate at high temperatures results into increase in the crystallinity benefiting its usage in the field of dosimetry [31]. Determination of the kinetic parameters associated with the TL glow curves is important for studying glow curve structures, trapping levels and kinetics. Different methods such as, Computerized Glow Curve Deconvolution (CGCD), Initial Rise (IR) and Various Heating Rate (VHR) method were used to evaluate the kinetic parameters [32]. Kinetic parameters determined using these methods were found to be approximately the same showing consistency in the approach.

Rare earth (lanthanides) doped aluminate materials have attracted attention of researchers due to their greater chemical stability and strong emission properties in the visible region of the electromagnetic spectrum [33–35]. Emission in rare earth impurities doped aluminate hosts span over the whole range of visible spectrum from blue to infra-red for their various applications including solid state lighting, display devices, up-conversion and quantum cutting, high-temperature monitoring (optical thermometry) using luminescence techniques, etc. [36–41]. Most of the rare-earth impurities show variable oxidation states. They can exist in

different (+2, +3 and +4) oxidation states in the same host material and their ionic states could be changed by redox reactions on annealing these phosphors materials in reducing/oxidizing atmospheres for tuning their chromaticity and colour coordinates. The sensitivity of the TLD phosphor materials could also be improved by energy transfer by co-doping and redox reactions [25, 42–45]. In this paper, we have used dysprosium as an impurity for doping the host material. The previous reported result of dysprosium suggests strongest emission for the transition ${}^4\text{F}_{9/2} \rightarrow {}^6\text{H}_{13/2}$ of Dy^{3+} ion. Three distinct emission peaks, which are mostly found at 493 nm (blue), 584 nm (yellow), and 680 nm (red) in the emission spectra, are primarily responsible for the Dy^{3+} transitions such as ${}^4\text{F}_{9/2} \rightarrow {}^6\text{H}_{15/2}$, ${}^4\text{F}_{9/2} \rightarrow {}^6\text{H}_{13/2}$, and ${}^4\text{F}_{9/2} \rightarrow {}^6\text{H}_{11/2}$, respectively [35].

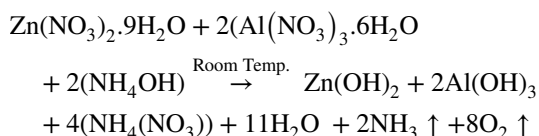
In this paper, we have emphasized on the TL properties of the dysprosium doped zinc aluminate phosphor material due to its good TL characteristics. Different chemical and physical methods are available to prepare the phosphor material, such as, co-precipitation, hydrothermal, combustion, sol–gel, thermal plasma, etc. to prepare the material in micro- and nanocrystalline forms [8, 9, 20, 35, 42, 46–49]. These methods have some advantages and disadvantages. In the present study, materials doped with different impurity concentrations (0.0–1.0 M%) were prepared by using a hybrid route. Firstly, the materials in intermediate states were prepared by co-precipitation method and then sintered at high temperature to form a single phase. Thus, the materials were annealed at different temperatures in the range of 400–1600 °C for 2.0 h. The synthesized phosphor materials were characterized by using various characterization techniques such as, X-Ray Diffraction (XRD), Fourier transformed infrared spectroscopy (FTIR), UV–visible spectroscopy, Field Emission Scanning Electron Microscopy (FESEM), Thermo-gravimetric (TG) and differential thermal analysis (DTA) and Photoluminescence (PL). Using ${}^{60}\text{Co}$ gamma-rays radioactive source, the phosphor was irradiated for different doses and thermoluminescence (TL) glow curves were recorded. The kinetic parameters of the TL glow curve were investigated using CGCD, IR and VHR methods.

Experimental

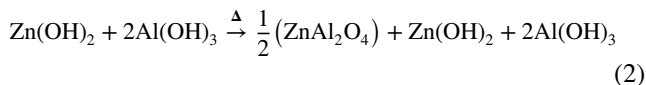
Synthesis of ZnAl_2O_4 : Dy^{3+}

The rare earth doped zinc aluminate phosphor can be prepared by using variety of chemical and physical techniques. The co-precipitation method was used to synthesize ZnAl_2O_4 : Dy^{3+} ($x = 0.0$ – 1.0 M %) phosphor due to its simplicity and time saving characteristics [50, 51]. Precursors of

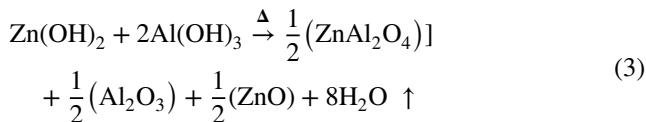
the Analytical Reagent (AR) grade such as $\text{Zn}(\text{NO}_3)_2 \cdot 6\text{H}_2\text{O}$ (HPLC (99.99%)), $\text{Al}(\text{NO}_3)_3 \cdot 9\text{H}_2\text{O}$ (HPLC (99.99%)), NH_4OH (HPLC (99.99%)) and Dy_2O_3 (Alfa-Aesar (99.99%)) were used in stoichiometric ratio. In order to synthesize $\text{ZnAl}_2\text{O}_4 \cdot \text{Dy}^{3+}$ phosphor, appropriate amounts of nitrates, and dysprosium were dissolved in the distilled water which was followed with constant stirring at room temperature for 2.0 h. Further, ammonia was added to the homogeneous and transparent mixture, until the pH of the solution was found to be 10.0. The resulted solution with white co-precipitate was filtered out at 2500 rpm by centrifuging and washing it using distilled water for several times. To evaporate the water content and pollutants, the centrifuged mixture was then dried in an oven for 24 h at 150 °C. The pristine material was sintered at different temperatures in air to get the material in the desired single ZnAl_2O_4 phase while considering the following equations [35, 50, 51]. Equation 1 indicates that the starting nitrate ingredients when treated with ammonium hydroxide get converted to their hydroxides.



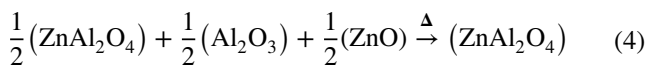
Finally, the synthesized powder was annealed in air at different temperatures ranging from 400 to 1600 °C for 2.0 h in high temperature tubular furnace. The heating as well as the cooling rate was 2.0 °Cs⁻¹. Equation (2) denotes the intermediate reaction for the phosphor annealed between 400 °C and 800 °C.



Equation (3) denotes the intermediate reaction for the phosphor annealed between 800 °C and 1400 °C,



while, Eq. (4) denotes the final reaction for the phosphor annealed at 1600 °C, where a single phase of ZnAl_2O_4 phosphor was obtained.



Annealed materials were then grinded to obtain the phosphor in the powder form. The prepared samples were further characterized by different characterization techniques and the intermediate phases were confirmed by comparing the XRD patterns with the JCPDS data of these phases (Sect. "X-ray Diffraction"). To investigate the TL properties,

the grinded powder samples were exposed to different doses of ⁶⁰Co gamma source.

Characterization techniques

Using Cu-target (Cu-K α = 1.54 Å) as X-ray source availed on the Bruker AXS D-8 Advance X-ray Diffractometer, the structural characteristics of the prepared samples were investigated. The employed voltage, current, scanning step and step size were 40 kV, 40.0 mA, 1.0 s/step, and 0.02 degree, respectively. Also, Field Emission Scanning Electron Microscope (FESEM) (JEOL JSM-6360A) equipped with an energy-dispersive X-ray spectrometer (EDS) was used to conduct the morphological and compositional analyses. To conduct this study, around 0.5 mg of the sample was sonicated in the presence of ethanol (10 ml) to attain a dispersive solution. A drop of the solution was put by a dropper onto a glass substrate and further dried by using IR lamp to form a layer of the material. The samples, thus, prepared were used for FESEM/EDS study. FTIR (JASCO FTIR 6100) spectroscopy technique was used to examine the functional groups of the $\text{ZnAl}_2\text{O}_4 \cdot \text{Dy}^{3+}$ (0.2 M%, 1600 °C) phosphor material in the region of 4000–400 cm⁻¹. Resolution of 2.0 cm⁻¹, scanning speed of 2.0 mm/sec, and an aperture of 5.0 mm were the applied constraints. In order to achieve good IR transmittivity, KBr was mixed with the sample in the ratio of 8:2. The phosphor material $\text{ZnAl}_2\text{O}_4 \cdot \text{Dy}^{3+}$ (0.2 M%) annealed at 1600 °C was also characterized by UV–visible spectroscopy (model V-770 JASCO) using an integrating sphere (ISN-923) powder sample holder (PSH-002) attachments for recording diffused reflectance spectra. For which the data interval of 0.5 nm, continuous scanning speed of 400 nm/min were the applied constraints. A dried KBr-pellet was used as reference material for the reflectance. TG–DTA analysis was carried out on Hitachi STA 7300 instrument in the presence of argon gas atmosphere. The TG–DTA curves were recorded in the temperature range of 10–900 °C with a heating rate of 20 °C min⁻¹. PL emission and excitation spectra were obtained with the help of Horiba Scientific fluorescence spectrophotometer (model PTI QM-8450-11-C system # 3560). For TL study, the samples in the powder form were preirradiated for different doses by using ⁶⁰Co gamma source located at the Savitribai Phule Pune University. TL measurements were recorded at least three times by using a computerized research TLD-reader (Nucleonix Systems Pvt. Ltd., India, Model TL1009I). The TLD-reader consists of a 25 mm PMT with ultra-low dark count as a photodetector and a PID temperature controller and programmer for linear heating. The PMT was operated at a voltage of 800 V and current in the range of pico- to microamperes. Approx. 5.0 mg of the samples were taken each time for recording the TL glow curve with linear heating rate of 5.0 °C/s. TL intensity was normalized by exact mass of the sample

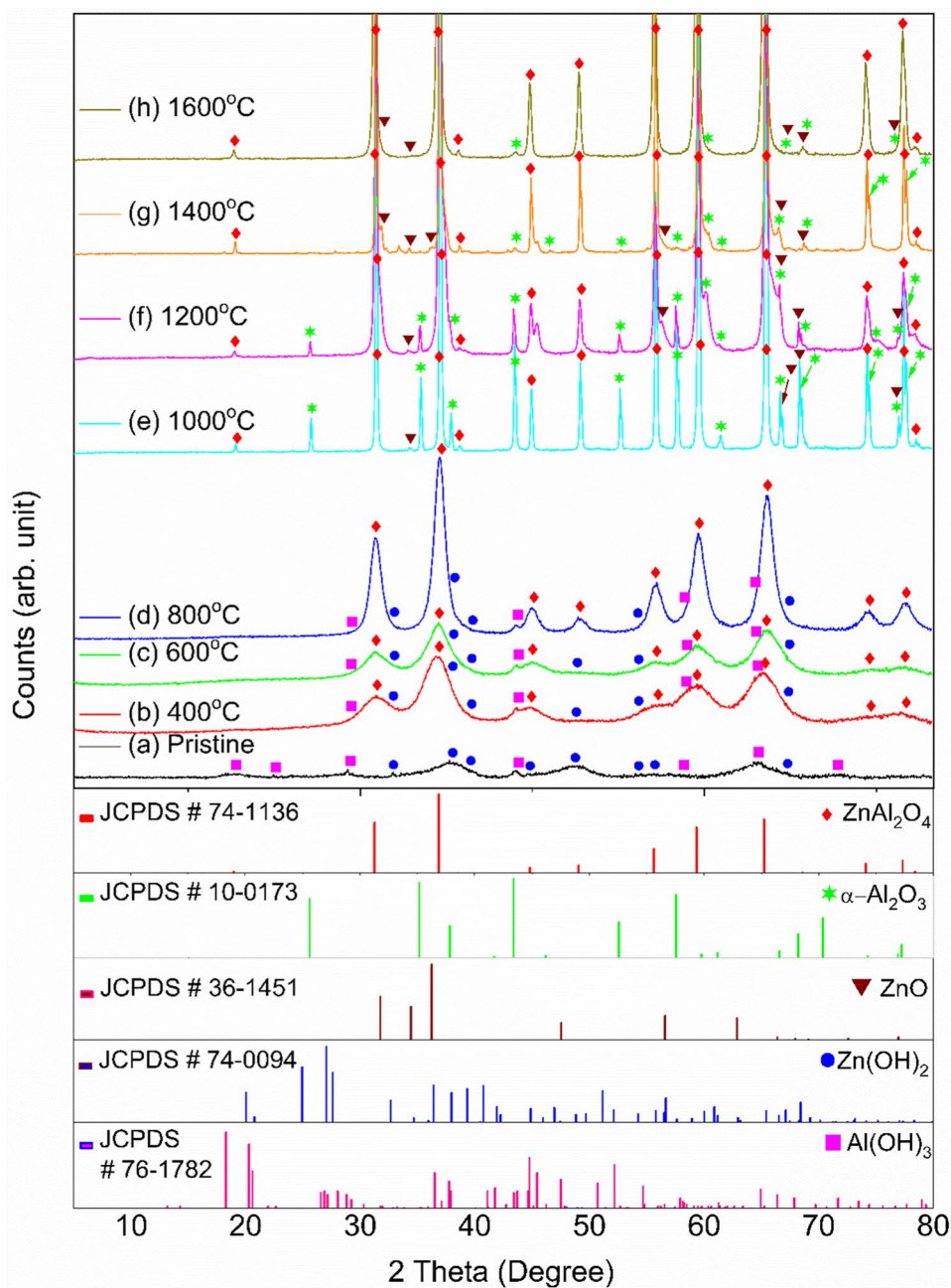
measured each time. In order to explore the reusability study, the optimized phosphor material ($\text{ZnAl}_2\text{O}_4:\text{Dy}^{3+}$ (0.2 M%), 1600 °C) was mixed with a small amount of polytetrafluoroethylene (Teflon) powder in the mass ratio of 10:1 to make a pellet using a hydraulic press for better handling. The pellet was irradiated for a 10.0 Gy test dose of gamma rays from ^{60}Co radioactive source to record the TL glow curve. The TL glow curve was recorded up to 400 °C and the procedure was repeated several times.

Results and discussion

X-ray Diffraction

The XRD patterns of the materials annealed at different temperatures are shown in Fig. 1a–h. XRD pattern of the material prepared by the coprecipitation method and dried at 150 °C is shown in Fig. 1 (pattern a). The XRD pattern was compared with the standard XRD data of ZnAl_2O_4 (JCPDS file # 74-1136) and it was found that none of the peaks matched with the data in this file. It was, therefore, thought

Fig. 1 X-ray diffraction patterns of the materials: **a** as prepared by coprecipitation method, **b** annealed at 400 °C, **c** annealed at 600 °C, **d** annealed at 800 °C, **e** annealed at 1000 °C, **f** annealed at 1200 °C, **g** annealed at 1400 °C and **h** annealed at 1600 °C, respectively. The stick plots of different phases occurring at different annealing temperatures are also plotted from the data in their respective JCPDS files and given here for ready reference. The various phases that are occurring at different annealing temperatures are $\text{Zn}(\text{OH})_2$, $\text{Al}(\text{OH})_3$, ZnO , $\alpha\text{-Al}_2\text{O}_3$, and ZnAl_2O_4 . No separate phase of the Dy-impurity has been observed at any stage of synthesis or annealing showing that the impurity is dispersed evenly in the host matrix. The broad peaks in patterns (a–d) were deconvoluted (not given here for clarity) by a Gaussian function to confirm the occurrences of peaks corresponding to different phases. (Color figure online)



that some intermediate states (phases) of the constituent elements, i.e., $\text{Al}(\text{OH})_3$ and $\text{Zn}(\text{OH})_2$, as given in Eq. (1) might have been formed. Therefore, experimental data was compared with the standard data in JCPDS Card No. 74-0094 and JCPDS Card No. 76-1782 for probable hydroxide materials. It was discovered that the diffraction peaks of this material matched with the XRD peaks appearing at around 18.34° , 22.69° , 28.85° , 44.33° , 58.06° , 64.38° , 71.30° belonging to the (200), ($\bar{1}$ 11), ($\bar{2}$ 02), (313), ($\bar{2}$ 24), (331), (226) hkl-planes, respectively, of the monoclinic phase (space group $\text{P}12_1/\text{c}1$) of the $\text{Al}(\text{OH})_3$ compound and were symbolized by (■) whereas, the peaks located around 32.67° , 37.96° , 39.32° , 44.88° , 48.82° , 54.26° , 55.80° , 67.12° denoted by (●) and belonged to (121), (012), (201), (221), (032), (310), (240), (312) planes of the orthorhombic phase ($\text{P}2_1 \bar{2} \bar{1}$) of the $\text{Zn}(\text{OH})_2$ compound. The phosphor annealed at different temperature ranging from 400°C to 800°C . The XRD peaks (symbolized by (◆)) patterns (b–d) showed that these phases get converted to face centered cubic (FCC) phase of the ZnAl_2O_4 though the traces of the hydroxide phases of zinc and aluminum could still be observed in this temperature range. It is interesting to see that annealing the material at still higher temperature ($\sim 1000^\circ\text{C}$) some new XRD peaks (pattern e) appeared in addition to that of ZnAl_2O_4 phase (Table 1). When these peaks were compared with the JCPDS data (JCPDS file # 36-1451 and 10-0173) it matched perfectly revealing that some of these peaks symbolized by (▼) correspond to wurtzite phase having hexagonal symmetry (space group $\text{P}6_3\text{mc}$) of ZnO (peaks appearing at around 2θ values 31.77° , 34.42° , 36.25° , 56.60° , 66.38° , 69.10° , 76.96° belonging to (100), (002), (101), (110), (200), (201), (202) planes) and the others symbolized by (★) correspond to corundum like orthorhombic phase (space group Pbcn) of the $\alpha\text{-Al}_2\text{O}_3$ (peaks appearing at around 2θ values 25.58° , 35.14° , 37.79° , 43.36° , 52.55° , 57.52° , 59.77° , 61.35° , 66.55° , 68.20° , 74.27° , 76.88° , 77.23° belonging to (012), (104), (110), (113), (024), (116), (211), (018), (214), (300),

(208), (1010), (119) planes). It seems that either the ZnAl_2O_4 phase might be getting separated in to these phases or the traces of the earlier remaining hydroxide phases of zinc and aluminum might be getting converted in to their respective oxide phases. However, on annealing the phosphor further at higher temperatures ($1200\text{--}1600^\circ\text{C}$), the XRD patterns (f–h) exhibited that the individual oxide phases of ZnO and $\alpha\text{-Al}_2\text{O}_3$ started diffusing evenly to form a single-phase ZnAl_2O_4 as shown in pattern (h). The rise in the intensity as well as sharpness of the XRD peaks with the annealing temperature increasing suggested that there is an increase in the crystallinity and grain size of the $\text{ZnAl}_2\text{O}_4\cdot\text{Dy}^{3+}$ phosphor on annealing [35]. No separate phase of the Dy-impurity has been observed at any stage of synthesis or annealing showing that the impurity is dispersed evenly in the host matrix. The lattice parameters were also calculated for the $\text{ZnAl}_2\text{O}_4\cdot\text{Dy}^{3+}$ (0.2 M%) phosphor annealed at 1600°C and are given in Table 1. The lattice parameters (a, b, c) were determined by using following Eq. 5 for a cubic lattice.

$$d = \frac{a}{\sqrt{h^2 + k^2 + l^2}} \quad (5)$$

Field emission scanning electron microscopy (FESEM)

The morphological study of the synthesized phosphor was carried out using FESEM technique. Figure 2a–e shows FESEM images of the materials annealed at different temperature. The FESEM images revealed the development of soft aggregates of the particles of nanometre sizes. The particles get aggregated to bigger sizes on annealing at higher temperatures [48, 49]. Figure 3a–e represents the histogram images of the particle size distribution of the materials annealed at different temperature. The average particle size of the materials annealed at different temperature

Table 1 Calculated values of the lattice parameter of $\text{ZnAl}_2\text{O}_4\cdot\text{Dy}^{3+}$ (0.2 M%, 1600°C) phosphor

Sample	2θ (degree)	h k l	FWHM (radian)	a (\AA) (Cubic Phase)
$\text{ZnAl}_2\text{O}_4\cdot\text{Dy}^{3+}$ (0.2 M%, 1600°C)	19.08	111	0.00320	8.04
	31.14	220	0.00414	8.11
	36.85	311	0.0045	8.08
	44.87	400	0.00452	8.07
	49.24	331	0.00458	8.06
	55.77	422	0.00503	8.06
	59.46	511	0.00546	8.07
	65.31	440	0.00613	8.07
	74.19	620	0.00585	8.07
	77.38	533	0.00669	8.08

are represented in Table 2 and are also shown graphically in Fig. 3f. The as prepared material has an average particle size of 107 nm. The grain sizes of the materials were found to increase with the increasing annealing temperature as reported earlier in the literature [52]. The average particle size of the finally prepared in single phase of $\text{ZnAl}_2\text{O}_4\text{:Dy}^{3+}$ (0.2 M %) after annealing at 1600 °C was found to be approx. 261 nm from the FESEM images.

Fourier transformed infrared spectroscopy (FTIR) and energy dispersive spectroscopy (EDS)

The FTIR absorption spectra of the pristine (as prepared) and the material annealed at 1600 °C is as shown in the Fig. 4a (spectra (i) and (ii)). Various absorption bands appearing in these spectra could be assigned to different (rotational, vibrational or stretching) modes of functional groups present. Highly intense band around 3722 cm^{-1} in the pristine material could be attributed to the stretching oscillations of the O–H functional group indicating the presence of hydroxides of the constituent elements formed during synthesis by coprecipitation method as predicted in Eq. (1) [48, 50, 51]. The other bands appearing in the frequency range of $2820\text{--}3100\text{ cm}^{-1}$ could be assigned to stretching of the C–H group, similarly, bands 1758 and 1372 cm^{-1} are due to C=O stretching and rocking. These functional groups might be due to environmental CO_2/CO present due to pollution. An absorption band appearing at around 1562 cm^{-1} could be assigned to N–O asymmetric stretching and yet another

band appearing at around 1303 cm^{-1} could be attributed to N–C stretching. The presence of these groups may be due to ammonium nitrate and residues produced during synthesis which later get eliminated by decomposition during annealing. Several bands in the frequency range of $1200\text{--}400\text{ cm}^{-1}$ in both the FTIR spectra could be assigned to vibrational, rotational and stretching modes of Zn–O, Zn–O–Zn, Al–O, Al–O–Al groups due to the formation of hydroxides, individual oxides and mixed oxide on annealing of the pristine material. It could, however, be observed in these spectra that all the absorption band corresponding to the hydroxide and other organic groups diminished on annealing at 1600 °C. For the phosphor annealed at 1600 °C, Very weak bands in the frequency range ($1371\text{--}1562\text{ cm}^{-1}$) related to C–H and C=O groups may be occurring due to adsorption of atmospheric CO_2/CO and formation of hydrogen bonding due to adsorption of water molecules.

The elemental composition analysis of $\text{ZnAl}_2\text{O}_4\text{:Dy}^{3+}$ (0.2 M%) phosphor annealed at 1600 °C was obtained from the energy dispersive spectroscopy (EDS) and is represented in Fig. 4b. The result revealed that the $\text{ZnAl}_2\text{O}_4\text{:Dy}^{3+}$ compound exhibited three prominent peaks corresponding to Zn, Al, O elements. Small crests of the Dysprosium element confirmed the presence of Dy^{3+} ions in the matrix. Table annexed to Fig. 4b shows the atomic percentage of the $\text{ZnAl}_2\text{O}_4\text{:Dy}^{3+}$ (0.2 M%) phosphor annealed at 1600 °C. Absence of the atomic percentage for dysprosium ion was noted; which may be due to the less doping concentration

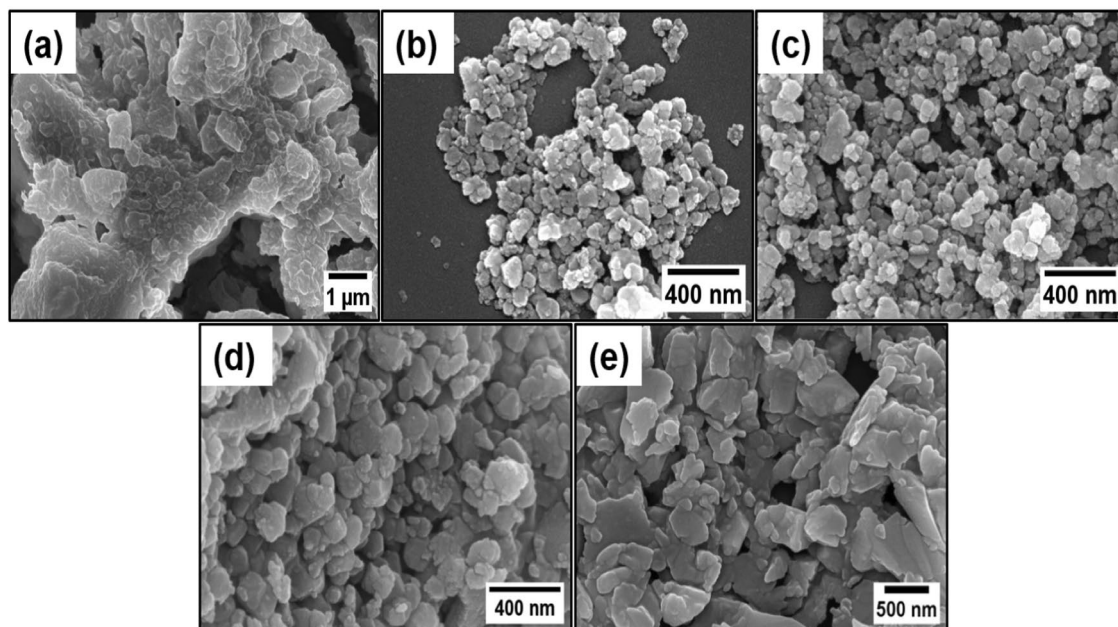


Fig. 2 FESEM images of $\text{ZnAl}_2\text{O}_4\text{:Dy}^{3+}$ (0.2 M %) phosphor **a** as prepared by coprecipitation method and annealed at **b** 400 °C, **c** 1000 °C, **d** 1400 °C and **e** 1600 °C, respectively. (Color figure online)

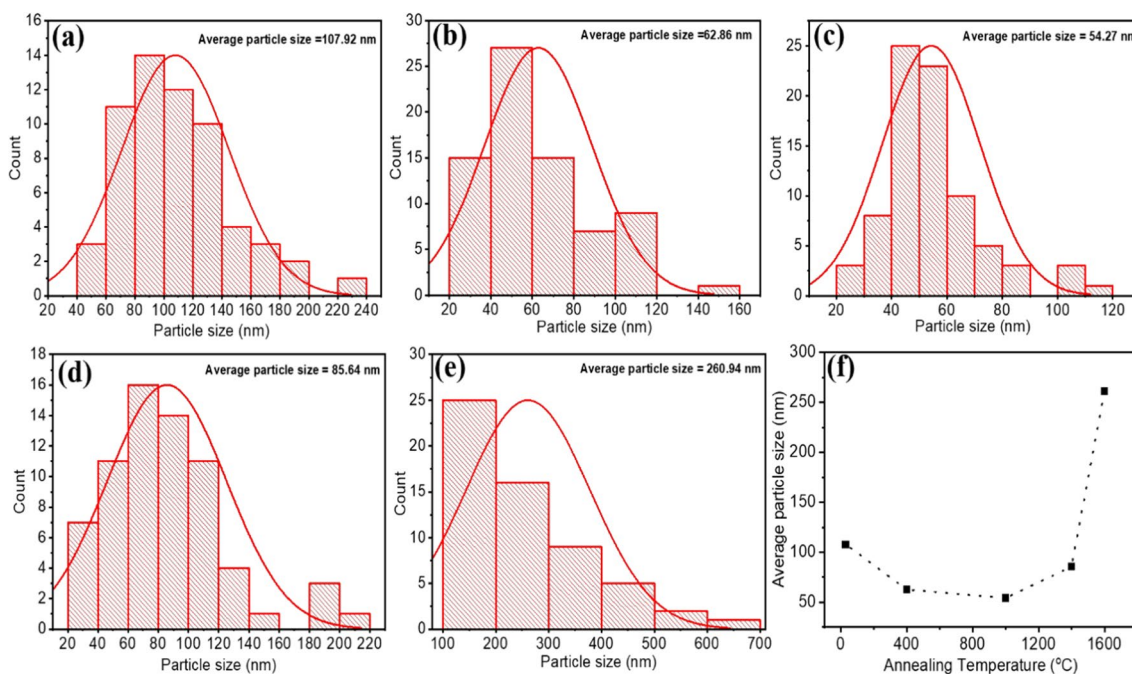


Fig. 3 a–e histogram graph of grain sizes distribution of the $\text{ZnAl}_2\text{O}_4:\text{Dy}^{3+}$ (0.2 M %) phosphor a as prepared and which was further annealed at b 400 °C, c 1000 °C, d 1400 °C and e 1600 °C

Table 2 Average particle sizes of the as prepared $\text{ZnAl}_2\text{O}_4:\text{Dy}^{3+}$ (0.2 M%) phosphor annealed at different temperature

Sr. No	Annealing temperature (°C)	Average particle sizes (nm)
1	as prepared	107.92
2	400	62.88
3	1000	54.27
4	1400	85.64
5	1600	260.94

(0.2 M%) of dysprosium ions. However, EDS spectra showed the presence of the peak for dysprosium element.

UV–visible spectroscopy analysis

UV–visible diffused reflectance spectra of the $\text{ZnAl}_2\text{O}_4:\text{Dy}^{3+}$ (0.2 M%) phosphor material annealed at 1600 °C was measured at RT in the range of 200–1000 nm and is shown in the Fig. 5. A strong peak around 277 nm was observed for $\text{ZnAl}_2\text{O}_4:\text{Dy}^{3+}$ phosphor which may be due to ... of the material [53]. The band gap energy (E_g) of the $\text{ZnAl}_2\text{O}_4:\text{Dy}^{3+}$ sample was determined using the well-known Tauc relation is given by Eq. (6)

respectively, and f variation of average particle sizes with annealing temperature. (Color figure online)

$$\alpha h\nu = (h\nu - E_g)^\lambda \quad (6)$$

where h is the Planck's constant, α is the Kubelka–Munk (K–M) absorption coefficient, and ν is the frequency. The extrapolation of the linear regions of the Tauc graph using the relation $(\alpha h\nu)^\lambda$ vs. $h\nu$ (Fig. 5, inset) is used to determine the value of the direct band gap E_g and was found to be 3.91 eV [54, 55].

Thermal analysis

The thermal behaviour of the sample was studied by using thermo-gravimetric (TG) and differential thermal analysis (DTA) method and is shown in Fig. 6a and b respectively. As the samples were prepared by the wet coprecipitation method, some water molecules might have been trapped inside and get released on heating contributing to the weight loss. Furthermore, as predicted in Eq. (1), there is formation of Zn and Al hydroxides in the process of coprecipitation and the decompose on subsequent heating huge weight loss due to release of large number of water molecules is expected as seen in TGA curve (curve i) of the as prepared material [55]. This process already occurs in case of the samples pre-annealed at different high temperatures and therefore the weight loss goes on decreasing with the annealing temperatures of the pre-annealed materials as seen in the other curves (ii–iv). No water molecules or other trapped

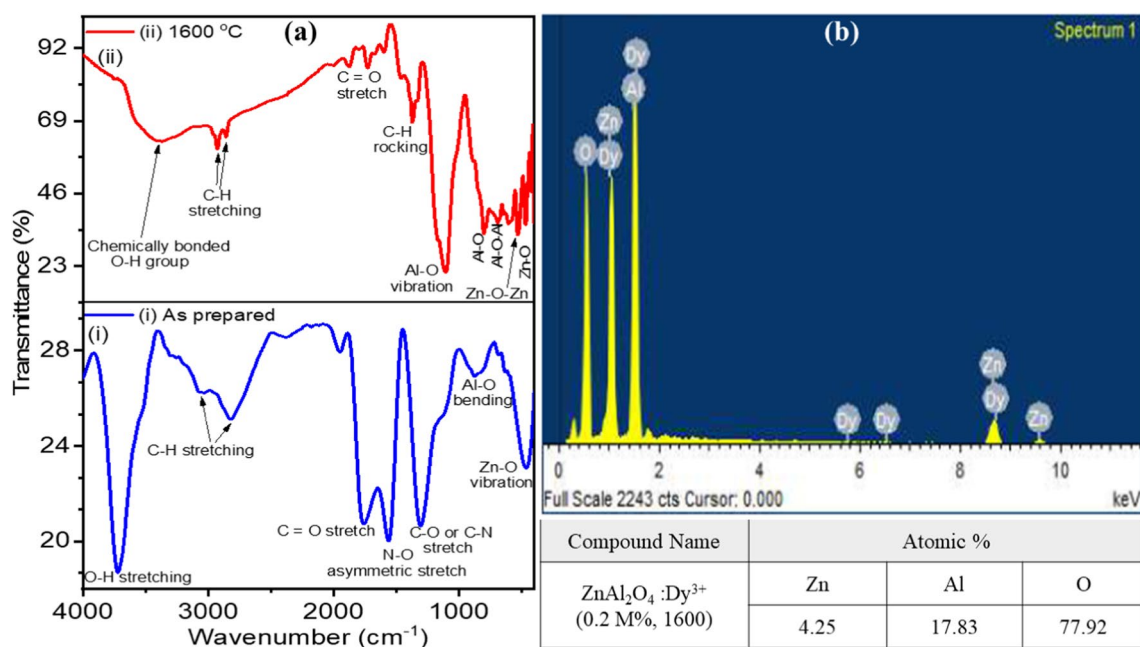


Fig. 4 **a** FTIR spectra of the as prepared material, **b** EDS spectra and percentage wise atomic composition of ZnAl₂O₄:Dy³⁺ (0.2 M%) phosphor annealed at 1600 °C. (Color figure online)

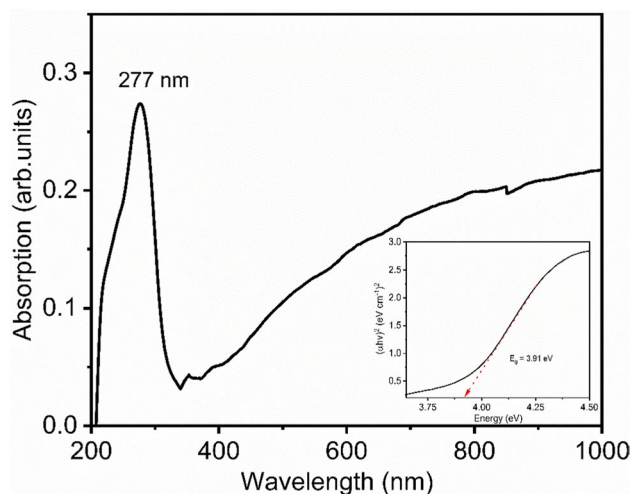


Fig. 5 Absorbance spectra and Tauc plot (inset) for ZnAl₂O₄:Dy³⁺ (0.2 M%) annealed at 1600 °C. (Color figure online)

gases could remain in the materials annealed above 1000 °C and thus the TGA curves become very much flat.

From the TGA curve, four regions of weight loss are observed for the as prepared sample. The first weight loss was found to be 7.69% at ~ 100 °C attributed to the removal of adsorbed/trapped water molecules from the sample [55]. In the second region, up to 20.55% of weight loss was observed in the range 150–330 °C, representing the loss of

the chemisorbed water [54]. The endothermic process led 5.78% weight loss was observed in the range of 330–470 °C. The peaks in the range of 330–470 °C in the DTA curve represented the desorption of adsorbed CO₂ and release of water molecules on decomposition of the intermediate hydroxides of Zn and Al. A small weight loss of 5.53% was observed in the fourth region with the exothermic peaks at 588–820 °C, associated to the formation of ZnAl₂O₄ at higher temperatures. The TGA curves in the Fig. 6a suggested that in as prepared sample there was around 40% weight loss. It was obvious, as some water molecules were present in the as prepared sample and do get released on heating which contribute to the weight loss. While the weight loss gradually decreases for the phosphor with increasing applied heat treatment and were found to be approximately 18%, 6%, 1%, 0.7% for the samples annealed at 400 °C, 800 °C, 1200 °C and 1600 °C respectively. DTA curves of the as prepared sample and that of annealed 600 °C show endothermic peaks at 100, 248, 813 and 900 °C, which indicate release of the adsorbed water and various gas molecules and the phase changes involved as given by Eqs. (1–4). However, not many changes could be observed in such curves of the samples annealed at higher temperatures as phase changes had already taken place during annealing and also as the DTA could not be taken at temperatures higher than 900 °C due to limitations of the equipment. The results were also found in correlation with the XRD analysis.

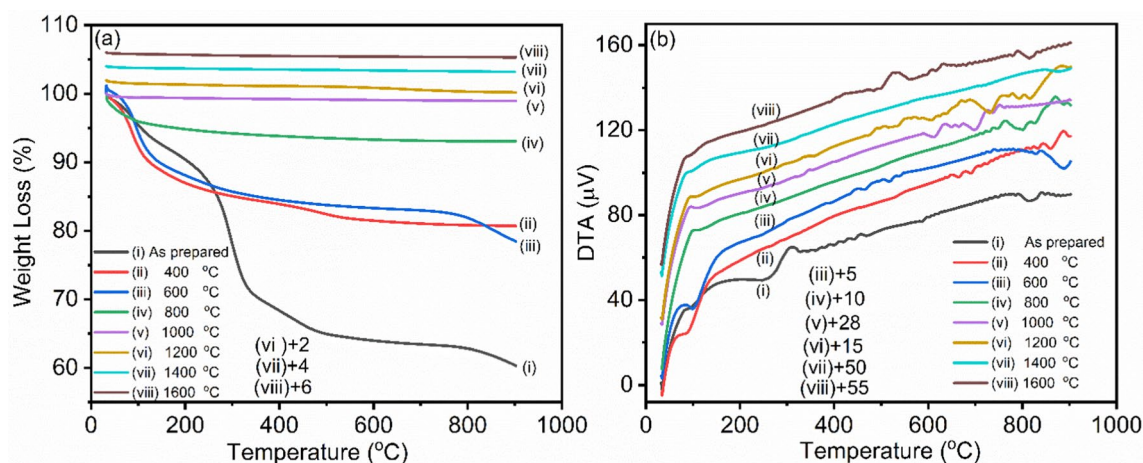


Fig. 6 aTGA and b DTA curves of the (i) as prepared $\text{ZnAl}_2\text{O}_4:\text{Dy}^{3+}$ (0.2 M %) phosphor and annealed at different temperatures (ii) 400 °C, (iii) 600 °C, (iv) 800 °C, (v) 1000 °C, (vi) 1200 °C, (vii) 1400 °C and (viii) 1600 °C. The ordinate is to be subtracted by the numbers near the curves to get the relative values of the parameters. (Color figure online)

Photoluminescence (PL)

The PL properties of the $\text{ZnAl}_2\text{O}_4:\text{Dy}^{3+}$ (0.2 M%) sample annealed at 1600 °C was investigated carefully. The excitation spectra of $\text{ZnAl}_2\text{O}_4:\text{Dy}^{3+}$ phosphor monitored at 481 nm is shown in the Fig. 7a. The spectra consisted of several excitation bands located in the region 290–450 nm due to the different transitions from the ground state (${}^6\text{H}_{15/2}$) to various excited states of Dy^{3+} ions. Spectra showed sharp excitation peak at ~343 nm corresponding to the ${}^6\text{H}_{15/2} \rightarrow {}^4\text{M}_{15/2}$, ${}^4\text{P}_{7/2}$ Dy^{3+} transitions and other peaks at 296 nm, 325 nm, 367 nm, 380 nm, 394 nm and 425 nm were assigned to the ${}^6\text{H}_{15/2} \rightarrow {}^4\text{D}_{7/2}$, ${}^6\text{H}_{15/2} \rightarrow {}^4\text{P}_{3/2}$, ${}^6\text{H}_{15/2} \rightarrow {}^4\text{D}_{7/2}$, ${}^6\text{H}_{15/2} \rightarrow {}^4\text{I}_{13/2}$, ${}^6\text{H}_{15/2} \rightarrow {}^4\text{M}_{21/2}$ and ${}^6\text{H}_{15/2} \rightarrow {}^4\text{G}_{11/2}$ transitions of the Dy^{3+} ion, respectively. Whereas, the peak at 280 nm was attributed to the charge transfer between O^{2-} and Dy^{3+} ions. The emission spectra of $\text{ZnAl}_2\text{O}_4:\text{Dy}^{3+}$ (0.2 mol%) sub-micron phosphor was monitored at an excitation of ~343 nm and is shown in Fig. 7b. Spectra contains one intense band at ~481 nm and other two relatively weak bands at ~564 nm and ~594 nm. The emission spectra of $\text{ZnAl}_2\text{O}_4:\text{Dy}^{3+}$ phosphor under 343 nm excitation exhibit sharp peaks in the blue (481 nm) and yellow (564 nm) region due to the ${}^4\text{F}_{9/2} \rightarrow {}^6\text{H}_{15/2}$ and ${}^4\text{F}_{9/2} \rightarrow {}^6\text{H}_{15/2}$ transitions, respectively. The blue emission was observed due to the magnetic dipole transition and yellow emission due to the hypersensitive electric dipole transitions [8]. The PL of the materials annealed at different temperatures was not given as the material was not formed in a single phase.

1400 °C and (vii) 1600 °C. The ordinate is to be subtracted by the numbers near the curves to get the relative values of the parameters. (Color figure online)

Thermoluminescence (TL)

Effect of annealing temperature and doping concentration

The effect of annealing on the TL glow curves of the $\text{ZnAl}_2\text{O}_4:\text{Dy}^{3+}$ (0.2 M%) phosphor material is as shown in Fig. 8. It could be noted here that no TL was observed in case of the as prepared material. It was as expected because it could be observed from Eq. (1) that during coprecipitation method the starting materials in their nitrate forms get converted in to hydroxides and OH^- radicals which are known as ‘killers of luminescence’ and thus no TL was observed [56, 57]. The as prepared sample (by coprecipitation method) did not exhibit the TL glow curve. From the XRD and TG–DTA analysis, it could be seen that the materials go through various phases as oxides of the ingredient compounds then mixed phases and finally after in the desired ZnAl_2O_4 phosphor material, therefore, the changes in their glow curve structures and the intensity was as expected and are clearly seen in Fig. 8 [58–60]. The inset of Fig. 8 suggested that there is increase in the TL intensity with the annealing temperature increasing and was found to be the maximum after annealing the $\text{ZnAl}_2\text{O}_4:\text{Dy}^{3+}$ (0.2 M%) phosphor material at 1600 °C.

Figure 9 shows the effect of doping concentration of Dy^{3+} ions on the TL glow curves of the $\text{ZnAl}_2\text{O}_4:\text{Dy}^{3+}$ (0.0–1.0 M%) phosphor material annealed at 1600 °C. The TL glow curves were recorded after irradiating the phosphor with a 10.0 kGy dose of gamma rays using ${}^{60}\text{Co}$ gamma source. The variation in the total TL intensity with doping concentration is also represented in the inset of Fig. 9.

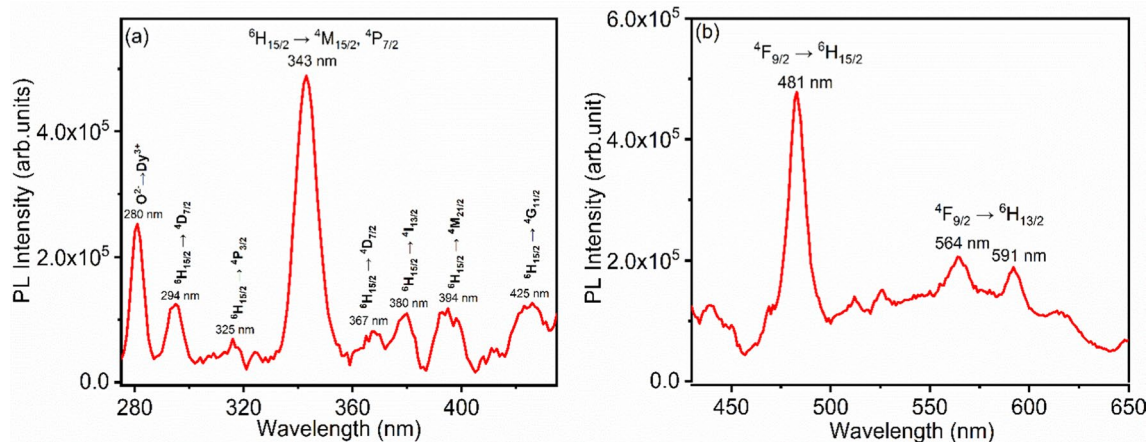


Fig. 7 PL spectra for $\text{ZnAl}_2\text{O}_4:\text{Dy}^{3+}$ (0.2 M%) phosphor material annealed at 1600 °C: **a** Excitation spectrum at the emission wavelength 481 nm, **b** Emission spectrum at the excitation wavelength

343 nm. The PL of the materials annealed at different temperatures was not given as the material was not formed in a single phase. (Color figure online)

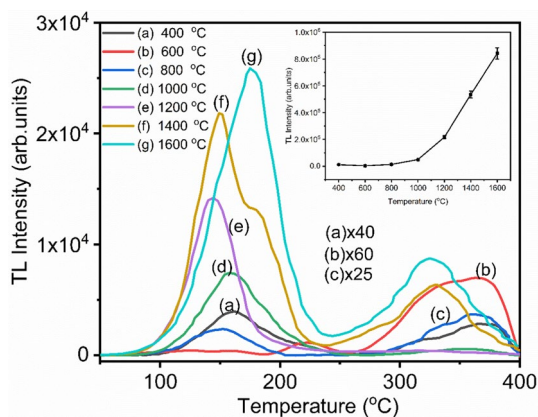


Fig. 8 TL glow curves of $\text{ZnAl}_2\text{O}_4:\text{Dy}^{3+}$ (0.2 M%) phosphor annealed at different temperature irradiated for a 10.0 kGy dose of a ^{60}Co gamma source. (Color figure online)

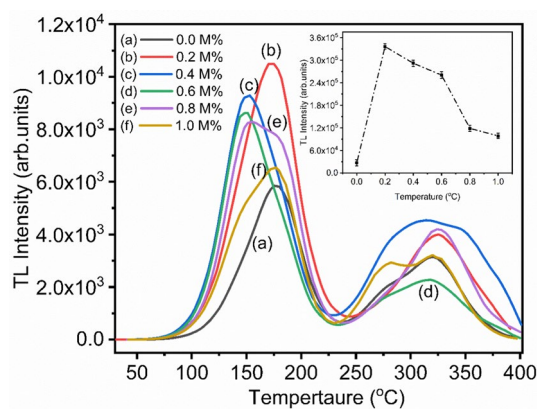


Fig. 9 TL glow curves of $\text{ZnAl}_2\text{O}_4:\text{Dy}^{3+}$ phosphor annealed at 1600 °C doped with different doping concentration (0.0–1.0 M%) of dysprosium ions irradiated for 10.0 kGy dose of a ^{60}Co γ -rays source. (Color figure online)

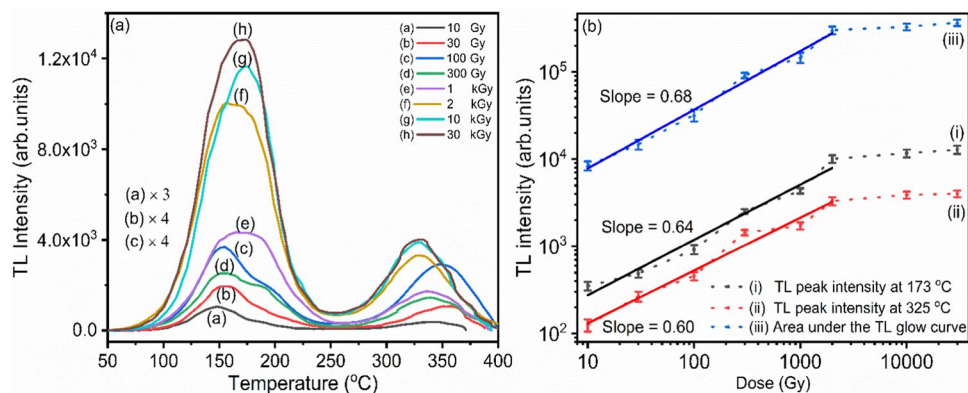
The undoped $\text{ZnAl}_2\text{O}_4:\text{Dy}^{3+}$ phosphor exhibited very low TL intensity. The highest TL intensity was noted for 0.2 M % doping concentration of Dy^{3+} ions and decreases significantly beyond this doping concentration. This is called concentration quenching and occurs due to interionic non-radiative transitions at higher doping concentrations [61].

Dose response

Figure 10a represents the TL glow curves of the $\text{ZnAl}_2\text{O}_4:\text{Dy}^{3+}$ (0.2 M%, 1600 °C) phosphor exposed to the different doses of gamma radiation (10.0 Gy to 30.0 kGy). No significant change in the TL glow curve structure and TL peak position was observed which clearly indicate that the phosphor shows first order kinetics. Figure 10b represent the dose response for the peak

173 °C, 325 °C as well as for the total TL intensity. It was found that the TL peak dose response for both the peaks and TL dose response by taking area under the curve into consideration showed sub-linear dose response in the range 10.0 Gy–2.0 kGy. Beyond 2.0 kGy the total TL intensity was observed to saturate with the increase in the gamma doses up to 30 kGy. The concentration of radiation-induced defects in such a high dose range (2.0–30.0 kGy) may have reached a threshold value, which had further led to the production of unstable defects (absorption centers) and structural alterations. This was the main reason for the saturation of the TL intensity over a certain absorbed dose. Also, the saturation in the TL intensity results from the production of

Fig. 10 **a** TL glow curves for the $\text{ZnAl}_2\text{O}_4:\text{Dy}^{3+}$ (0.2 M%, 1600 °C) phosphor at 1600 °C for different doses of a ^{60}Co γ -rays source, **b** dose response, curve (i) variation of the intensity with dose for 173 °C peak, curve (ii) variation of the intensity with dose for 325 °C peak, curve (iii) variation of the intensity with dose for area under the whole curve. (Color figure online)



an increasing number of tracks that overlap and may not provide additional TL intensity at very high doses [62].

Determination of number of peaks and locations in a TL glow curve by $T_{\text{max}}-T_{\text{stop}}$ Method The number and locations of the hidden peaks inside a complex TL glow curve can be shown by the $T_{\text{max}}-T_{\text{stop}}$ method. The $\text{ZnAl}_2\text{O}_4:\text{Dy}^{3+}$ (0.2 M%) phosphor annealed at 1600 °C for 2.0 h was irradiated for a dose of 10.0 kGy using ^{60}Co gamma source. 5.0 mg sample was heated with a linear rate ($5.0\text{ }^\circ\text{C s}^{-1}$) at an interval of 10 °C to a temperature T_{stop} corresponding to a position on the low-temperature tail of the first glow peak. In order to obtain the remaining glow curve, the same sample was then heated up to 400 °C, and the peak temperature (T_{max}) of the corresponding glow curve was recorded. Again, another 5.0 mg sample which was irradiated for the same dose was heated with same linear heating rate up to the new temperature (5.0 °C more than the previous temperature). This sample was now heated up to 400 °C to record the remaining glow curve and T_{max} was noted. This process was executed numerous times by raising the T_{stop} temperature by 5 °C above the previous attempt each time. T_{max} vs. T_{stop} graph is shown in Fig. 11, which exhibited staircase-like structure, with the T_{max} values corresponding to the steps (horizontally flat regions of the curve) representing the corresponding highest peak temperatures. Four hidden peaks were observed in the TL glow curve structure of the $\text{ZnAl}_2\text{O}_4:\text{Dy}^{3+}$ (0.2 M%, 1600 °C) phosphor at 173 °C, 196 °C, 325 °C, and 375 °C.

Deconvolution of TL glow curves and calculation of trapping parameters

TL glow curves of $\text{ZnAl}_2\text{O}_4:\text{Dy}^{3+}$ (0.2 M%, 1600 °C) phosphor exposed to different doses of gamma rays from ^{60}Co source (10.0 Gy–30.0 kGy) suggested no appreciable

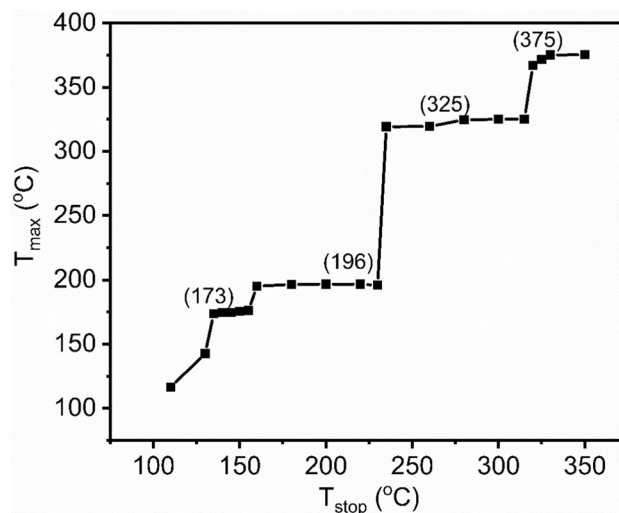


Fig. 11 Typical $T_{\text{max}}-T_{\text{stop}}$ graph for $\text{ZnAl}_2\text{O}_4:\text{Dy}^{3+}$ (0.2 M%) phosphor annealed at 1600 °C. (Color figure online)

change in the pöperatures. This shows that the peaks follow first order kinetics [61–63]. Therefore, the Computerized Glow Curve Deconvolution (CGCD) curve fitting method was used to deconvolute the glow curve suggested by Kitis at al. for the first order kinetics of glow curves [64]. The experimentally discovered TL glow curve was fitted for the kinetic analysis using CGCD method given by Pagonis et. al. [65]. The typical deconvoluted TL glow curves, theoretical curve along with the experimental TL glow curve of $\text{ZnAl}_2\text{O}_4:\text{Dy}^{3+}$ (0.2 M%) phosphor annealed at 1600 °C are shown in the Fig. 12. The deconvolution of TL glow curves, revealed significant overlap and good agreement between the theoretical and experimental glow curves (FOM 2.58%). Four peaks were discovered in a typical TL glow curve of $\text{ZnAl}_2\text{O}_4:\text{Dy}^{3+}$ phosphor which were located at around 173 °C, 196 °C, 325 °C and 375 °C.

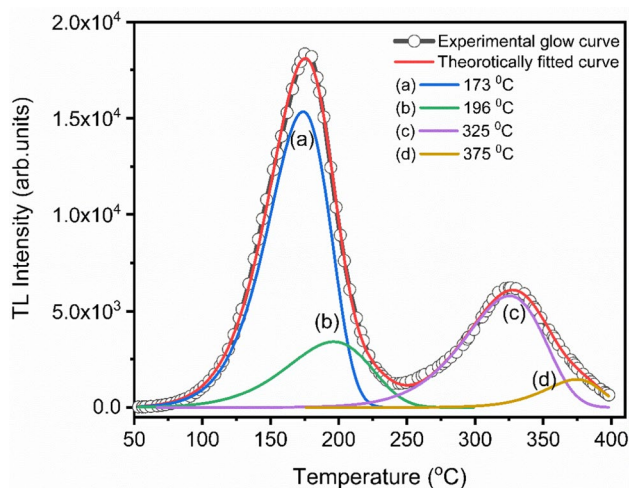


Fig. 12 Comparison between the experimental (—○—) and theoretically (—) fitted the TL glow curves of $\text{ZnAl}_2\text{O}_4:\text{Dy}^{3+}$ (0.2 M%) phosphor (annealed at 1600 °C for 2 h) irradiated for 10.0 kGy dose using ^{60}Co source. Deconvoluted single fitted glow curves, a, b, c, and d (—) can also be seen in the figure. (Color figure online)

For general order kinetics the function is given in Eq. (7)

$$I(T) = I_m b^{\left(\frac{b}{b-1}\right)} \exp\left(\frac{E}{kT} \frac{T - T_m}{T_m}\right) \left[(b-1) \frac{T^2}{T_m^2} \left(1 - \frac{2kT}{E}\right) \exp\left(\frac{E}{kT} \frac{T - T_m}{T_m}\right) + 1 + (b-1) \frac{2kT_m}{E} \right]^{\frac{-b}{b-1}} \quad (7)$$

For first order:

$$I(T) = I_m e^{\left[1 + \frac{E}{kT} \frac{T - T_m}{T_m} - \frac{T^2}{T_m^2} \exp\left(\frac{E}{kT} \frac{T - T_m}{T_m}\right) \left(1 - \frac{2kT}{E}\right) - \frac{2kT_m}{E}\right]} \quad (8)$$

Here, $I(T)$ is the TL intensity at temperature T (K), I_m is the maximum peak intensity, T_m is the temperature corresponding to maximum peak intensity I_m , E is the trap depth or the thermal activation energy (eV) needed to free the trapped electrons, and ' k ' is the Boltzmann's constant ($8.6 \times 10^{-5} \text{ eVK}^{-1}$).

The frequency factor ' s ' for first order kinetics is obtained from the Eq. (9).

$$S = \frac{\beta E}{kT_m^2} \exp\left(\frac{E}{kT_m}\right) \quad (9)$$

where, β is the linear heating rate.

To determine the kinetic parameters, Chen's set of empirical equations were used to compute the activation energy (E) and order of kinetics (b) of the deconvoluted illumination peaks of nanocrystalline ZnAl_2O_4 phosphor [66].

$$E_\alpha = C_\alpha \left(\frac{kT_m^2}{\alpha} \right) - b_\alpha (2kT_m) \quad (10)$$

with

$$\alpha = \tau, \delta, \omega$$

$$\tau = T_m - T_1, \delta = T_2 - T_m, \omega = T_2 - T_1,$$

$$C_\tau = 1.51 + 3.0(\mu_g - 0.42),$$

$$C_\delta = 0.976 + 7.3(\mu_g - 0.42),$$

$$C_\omega = 2.52 + 10.2(\mu_g - 0.42)$$

$$b_\tau = 1.58 + 4.2(\mu_g - 0.42),$$

$$b_\delta = 0,$$

$$b_\omega = 1.$$

To determine the order of kinetic, the form factor was calculated by using Eq. (11),

$$\mu_g = \frac{T_2 - T_m}{T_2 - T_1} \quad (11)$$

The form factor, μ_g , has a theoretical range of 0.42–0.52. For a peak with first order kinetics, form factor value is 0.42 and for second order kinetics the value is close to 0.52. In the Table 3; μ_g was found to be ~0.42 for all the deconvoluted glow curve, which verified that all the peaks obey first order kinetics. Furthermore, Balarin and Furetta offered the following factor (Eq. 12).

$$\gamma = \frac{T_2 - T_m}{T_m - T_1} \quad (12)$$

It ranges from 0.7 to 0.9 for first-order kinetics and from 1.05 to 1.20 for second order kinetics [66–68]. The activation energy or trapping depth (eV) values for different peaks ranged from 0.10 to 0.59 eV whereas, the values for the frequency factor ranged from 10^2 to 10^7 s^{-1} for $\text{ZnAl}_2\text{O}_4:\text{Dy}^{3+}$ (0.2 M%, 1600 °C) phosphor.

Various heating rate method

The kinetic characteristics of the $\text{ZnAl}_2\text{O}_4:\text{Dy}^{3+}$ phosphor were also determined using the Various Heating Rate (VHR) method. Figure 13a shows the TL glow curves of the $\text{ZnAl}_2\text{O}_4:\text{Dy}^{3+}$ (0.2 M%, 1600 °C) phosphor irradiated at 10 kGy, obtained at six different heating rates (1 °C/s to

Table 3 Kinetic parameters of $\text{ZnAl}_2\text{O}_4:\text{Dy}^{3+}$ (0.2 M%) phosphor irradiated for 10 kGy by CGCD, IR and VHR method

Peak temperature (°C)	Geometrical factor (μ_g)	Balarin parameter (γ)	Activation energy by CGCD (eV)	Activation energy by IR (eV)	Activation energy by VHR (eV)	Frequency factor by CGCD (s^{-1})	Frequency factor by IR (s^{-1})	Frequency factor by VHR (s^{-1})
173 ± 1	0.48	0.93	0.17 ± 0.008	0.16 ± 0.008	0.19 ± 0.009	$1.9 \pm 1 \times 10^5$	$2.1 \pm 1 \times 10^5$	$1.6 \pm 1 \times 10^5$
196 ± 1	0.49	0.98	0.11 ± 0.01	0.11 ± 0.005	–	$1.7 \pm 1 \times 10^2$	$3.1 \pm 1 \times 10^2$	–
325 ± 1	0.48	0.93	0.37 ± 0.01	0.37 ± 0.010	0.39 ± 0.01	$1.0 \pm 1 \times 10^5$	$1.3 \pm 1 \times 10^5$	$1.4 \pm 2 \times 10^5$
375 ± 1	0.42	0.74	0.59 ± 0.02	0.57 ± 0.020	–	$2.7 \pm 1 \times 10^7$	$5.3 \pm 1 \times 10^7$	–

6 °C/s). Kinetic parameters were calculated using the dependence of the peak position (T_m) on a heating rate (β). It was observed that when the linear heating rate increased, the TL peak intensity decreased. Also, the peaks were observed to shift towards high temperature range with increase in the linear heating rate. Chen introduced Eq. (10) for the case of general order kinetics in 1969 [66].

$$I_t = -\frac{dn}{dt} = s^1 n^b e^{-\frac{E}{kT}} \quad (13)$$

Eq. (13) is obtained for the case of first order kinetics where ($b=1$) in Eq. (13)

$$I_t = -\frac{dn}{dt} = nse^{-\frac{E}{kT}} \quad (14)$$

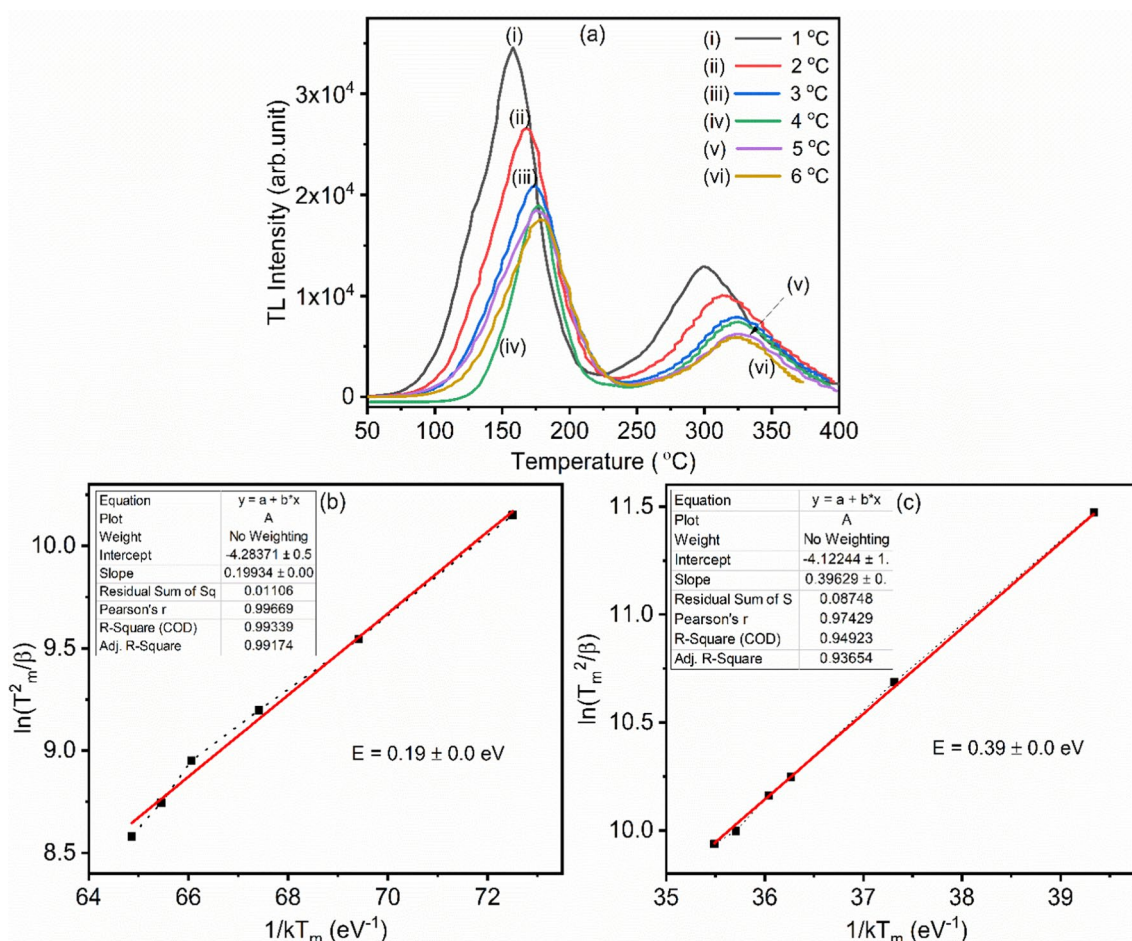


Fig. 13 a Glow curves of a 10 kGy irradiated $\text{ZnAl}_2\text{O}_4:\text{Dy}^{3+}$ (0.2 M%) phosphor annealed at 1600 °C measured at different heating rates, b and c Plot of $\ln\left(\frac{T_m^2}{\beta}\right)$ vs. $(1/kT_m)$ for the dominant and shoulder peak, respectively. (Color figure online)

Assuming a linear heating rate and integrating the Eq. (14) we get Eq. (15)

$$I(T) = -\frac{dn}{dt} = n_0 s e^{(-\frac{E}{kT})} e^{\left(-s \times \left(\frac{T}{T_0} \int_{T_0}^T e^{(-\frac{E}{kT})} dT \right) \right)} \quad (15)$$

Equation (16) was obtained by evaluating the derivative of Eq. (15) to zero, which gives the equation indicating the maximum of the glow peak.

$$\frac{\beta E}{kT_m^2} = s e^{(\frac{-E}{kT_m})} \quad (16)$$

We can derive the effort to escape factor (s) by rearranging the terms in Eq. (16).

$$s = \frac{\beta E}{kT_m^2} e^{(\frac{E}{kT_m})} \quad (17)$$

Taking \ln on both the side of the Eq. (16) we get,

$$\ln\left(\frac{\beta E}{kT_m^2}\right) = \ln(s) - \frac{E}{kT_m}$$

$$\ln\left(\frac{\beta E}{skT_m^2}\right) = -\frac{E}{kT_m}$$

$$\ln\left(\frac{skT_m^2}{\beta E}\right) = \frac{E}{kT_m}$$

$$\ln\left(\frac{T_m^2}{\beta}\right) = \frac{E}{kT_m} + \ln\left(\frac{E}{sk}\right) \quad (18)$$

The activation energy (E) was determined by slope of the straight line obtained from the graph in Fig. 13a and b, i.e., Plot of $\ln\left(\frac{T_m^2}{\beta}\right)$ vs. $(1/kT_m)$, whereas, the y-intercept in the graph also help us to obtain frequency factor (s) given by the Eq. (19)

$$s = \frac{E e^{\text{intercept}}}{k} \quad (19)$$

The kinetic parameters for the peaks at 173 and 325 °C could be found using the VHR method and are shown in the Table 3. Due to the inability of determining and identifying the peak position, the kinetic parameters for the other two peaks located around 196 and 375 °C could not be determined due to overlapping.

Initial rise method

The initial rise method was used to determine the kinetic parameters of $\text{ZnAl}_2\text{O}_4:\text{Dy}^{3+}$ (0.2 M%), phosphor annealed at 1600 °C. This method of was first suggested by Garlick and Gibson [69]. The sample (5.0 mg) was heated using the TL reader beyond the first TL peak's maximum, and was cooled. Another irradiated sample was heated upto a certain temperature such that the first peak was thermally cleaned. The sample was cooled and reheated beyond next peak's maximum to record the TL glow curve of second peak. The procedure was repeated for remaining peaks. It can be assumed that the number of trapped electrons in the low temperature tail of a TL peak remains approximately constant. For temperatures up to a cutoff temperature T_C , which is equivalent to a TL intensity I_C of less than 15% of the maximum TL intensity I_m , this method remains true [69, 70]. Figure 14 display the fractional glow curves of every peak (173 °C, 196 °C, 325 °C, and 375 °C) after thermally cleaning previous peak(s).

Equation (20) is the general order equation suggested by May and Patridge [70].

$$I(T) = -\beta \frac{dn}{dT} = Cs' n^b \exp\left(-\frac{E}{kT}\right) \quad (20)$$

In this case, the heating rate is represented by β , the pre-exponential component is s' , the scaling factor is C , and the concentration of trap carriers is denoted by n .

According to Rashedy for balance dimension suggested replacement of s' by $s/(N \cdot b^{-1})$ [71]

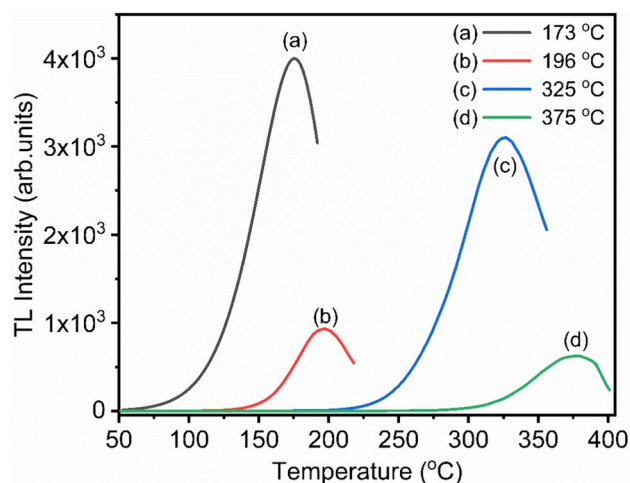


Fig. 14 Fractional-glow curves of a 10 kGy irradiated $\text{ZnAl}_2\text{O}_4:\text{Dy}^{3+}$ (0.2 M%) phosphor annealed 1600 °C recorded for the peaks **a** 173 °C, **b** 196 °C, **c** 325 °C and **d** 375 °C. (Color figure online)

$$I(T) = -\beta \frac{dn}{dT} = Csn \frac{n^b}{N^{b-1}} \exp\left(-\frac{E}{kT}\right) \quad (21)$$

When we substitute $b = 1$ for first order kinetics in Eq. (21), we obtain

$$I(T) = Csn \exp\left(-\frac{E}{kT}\right)$$

Equation (22) was produced by taking \ln on both sides of the equation.

$$\ln I(T) = \ln(Csn) - \frac{E}{kT} \quad (22)$$

Equation (22), which is expressed as $y = mx + c$, Fig. 15a–d displays the graph of $\ln I(T)$ vs $1/kT$ that was plotted for each of the following peak temperatures: 173 °C, 196 °C, 325 °C, and 375 °C. The activation energy (E) for each peak was determined by taking the negative slope of the straight line on the $\ln(I)$ vs. $(1/kT)$ graph.

From the graph of Fig. 15, intercept I is now expressed as

$$I = \ln Csn$$

Here, area under the curve, A was used in place of Cn , and the equation was rewritten as,

$$I = \ln(As)$$

$$I = \ln(A) + \ln(s)$$

$$\ln(s) = I - \ln(A)$$

$$s = \text{Antilog}[I - \ln(A)] \quad (23)$$

Kinetic parameters determined by IR method are represented in Table 3.

The uncertainty value of activation E was calculated by using standard deviation formula given in Eq. (24) and shown in Table 3.

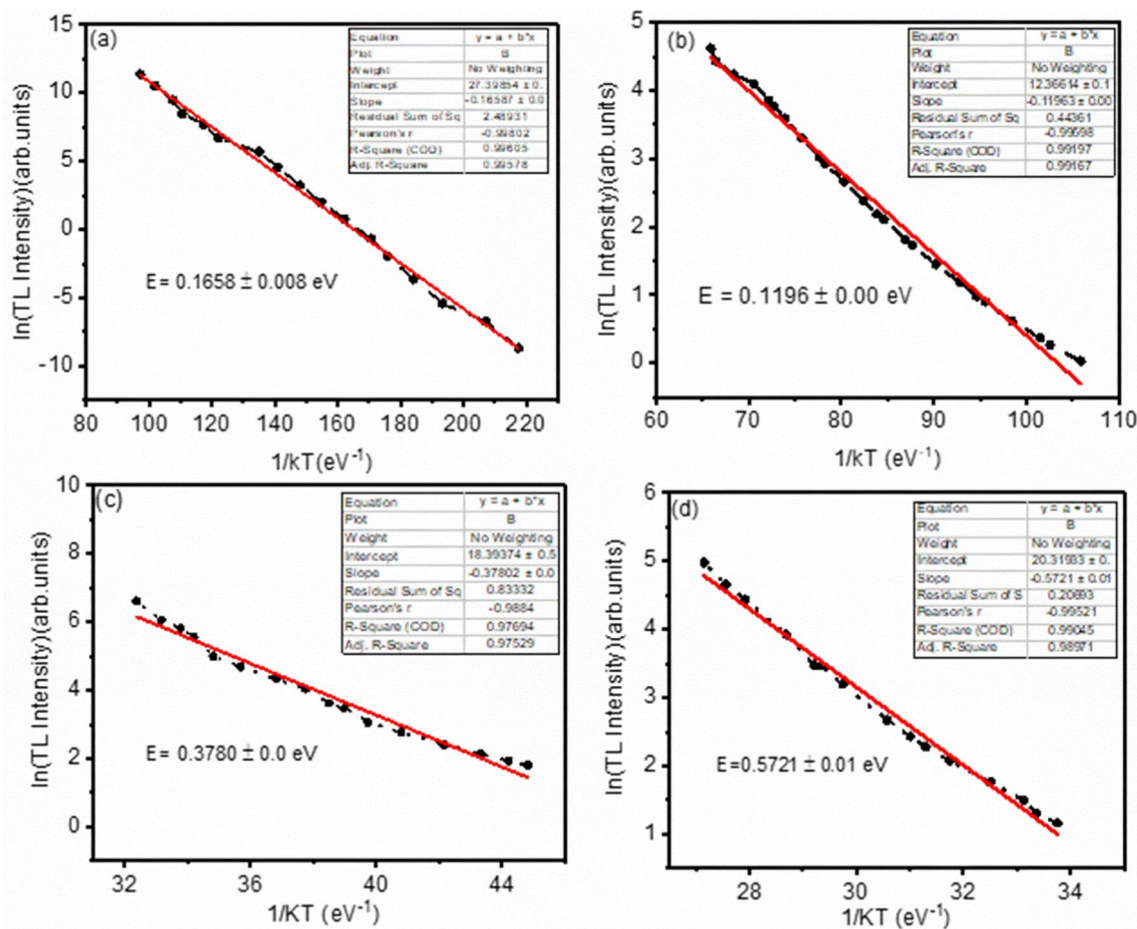


Fig. 15 Plot of $\ln(\text{TL Intensity})$ vs. $1/kT$ (of initial part) of the fractional glow curves of **a** 173 °C, **b** 196 °C, **c** 325 °C and **d** 375 °C of a 10 kGy irradiated $\text{ZnAl}_2\text{O}_4:\text{Dy}^{3+}$ (0.2 M%) phosphor annealed at 1600 °C respectively. (Color figure online)

$$S = \sqrt{\frac{\sum_{i=1}^N (x_i - \bar{x})^2}{N - 1}} \quad (24)$$

where S is the standard deviation of the sample, N is the number of observations, x_i are the observed values of a sample item and \bar{x} indicates the mean value of observation.

The activation energy and frequency factor found using the CGCD, IR and VHR methods, respectively, are shown in Table 3.

Reusability

One of the most important specifications for a good TLD phosphor is its ability to be reused. If a material's sensitivity or glow curve structure changes after it is being used once, it is not regarded as a suitable TL dosimeter; rather, these properties should not change even after the material has been exposed to radiation and has undergone multiple TL readouts. Therefore, the reusability study of the newly developed $\text{ZnAl}_2\text{O}_4:\text{Dy}^{3+}$ (0.2 M%, 1600 °C) phosphor was investigated. A 10.0 kGy dose of gamma radiation was delivered to the prepared pellet of $\text{ZnAl}_2\text{O}_4:\text{Dy}^{3+}$ phosphor to investigate its reusability property. Figure 16 shows the variation of total TL intensity of the phosphor with respect to the readout cycles. No noticeable variation in the TL sensitivity of the phosphor material was observed. The newly developed TLD phosphor is thus seen to have a very good reusability. This showed the material durability and has ability to be reused.

Comparison with standard TLD phosphor

The TL intensity of the synthesized $\text{ZnAl}_2\text{O}_4:\text{Dy}^{3+}$ (0.2 M%, 1600 °C) phosphor was compared with the

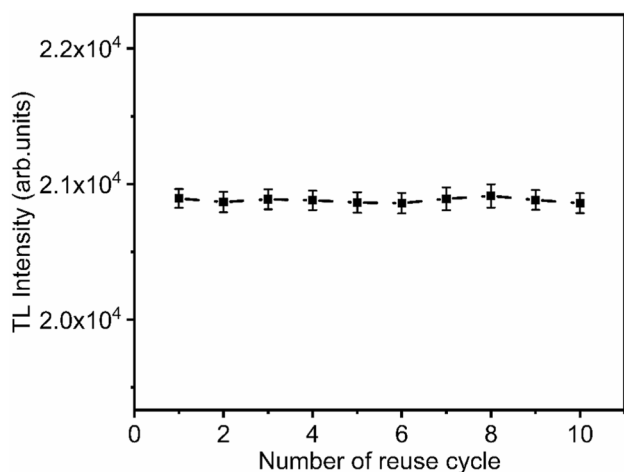


Fig. 16 Reusability of $\text{ZnAl}_2\text{O}_4:\text{Dy}^{3+}$ (0.2 M%, 1600 °C) phosphor irradiated for 10.0 kGy dose. (Color figure online)

standard existing TLD phosphor such as $\text{CaSO}_4:\text{Dy}$ (TLD-900) [72] and $\text{K}_2\text{Ca}_2(\text{SO}_4):\text{Eu}^{3+}$ (0.1 M%, 700 °C) nanophosphor [16]. All the phosphors were irradiated together for a dose of 1.0 kGy and the TL glow curves were recorded. The results are shown in the Fig. 17. The TL peak intensity of the $\text{ZnAl}_2\text{O}_4:\text{Dy}^{3+}$ phosphor was found to be around (1/25) and (1/17) times sensitive than the TLD-900 and $\text{K}_2\text{Ca}_2(\text{SO}_4):\text{Eu}^{3+}$ nanophosphor, respectively. Whereas, by the area under the curve method, the $\text{ZnAl}_2\text{O}_4:\text{Dy}^{3+}$ phosphor was noted to be around (1/23) and (1/8) times sensitive than the TLD-900, and $\text{K}_2\text{Ca}_2(\text{SO}_4):\text{Eu}^{3+}$ nanophosphor, respectively.

Fading

After being exposed to a 10.0 kGy dose of gamma irradiation, $\text{ZnAl}_2\text{O}_4:\text{Dy}^{3+}$ (0.2 M%, 1600 °C) phosphor material was kept in the dark at an ambient temperature (27 °C). After certain interval of time 5 mg of the stored sample was used each time to record the TL glow curve. The graph of total TL intensity vs. storage time for the peaks located around 173 °C and 325 °C were plotted separately and are shown in Fig. 18a and b respectively. The figure illustrated that the fading of the peak located at 173 °C was found to be 45% over first 7 days which is considered to be very high and not good for the dosimetry purpose. However, one shoulder peak present at higher temperature 325 °C can be used for dosimetry purpose due to low fading (8% in 7 days).

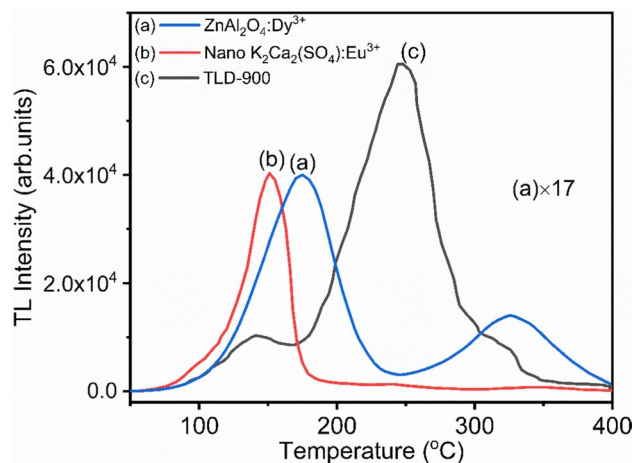


Fig. 17 Comparison of the TL Intensity of $\text{ZnAl}_2\text{O}_4:\text{Dy}^{3+}$ (0.2 M%, 1600 °C) with that of other known TLD phosphors, i.e., $\text{CaSO}_4:\text{Dy}$ (TLD-900) and $\text{K}_2\text{Ca}_2(\text{SO}_4)_3:\text{Eu}^{3+}$ (Nano), irradiated using 1.0 kGy gamma radiation dose from ^{60}Co radioactive source. (Color figure online)

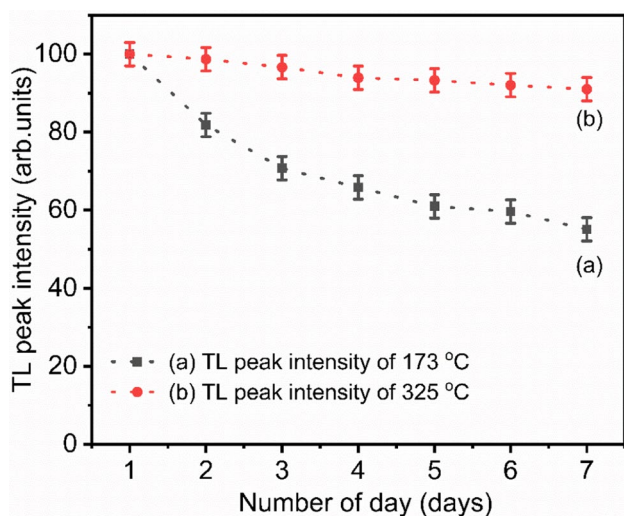


Fig. 18 Fading of the TL peak located at **a** 173 °C and **b** 325 °C for the $\text{ZnAl}_2\text{O}_4:\text{Dy}^{3+}$ (0.2 M%, 1600 °C) phosphor. The material in powder form was irradiated to 10.0 kGy dose of γ -radiation from ^{60}Co source, stored in dark at room temperature and TL was taken at different intervals of time. The intensity on Y-axis (ordinate) was normalized to find the fading directly in percentage. (Color figure online)

Conclusion

The $\text{ZnAl}_2\text{O}_4:\text{Dy}^{3+}$ (0–1 M%) phosphor was successfully synthesized using a co-precipitation route. The phosphor was found to exist in pure face centered cubic crystal structure when annealed at 1600 °C. The lattice parameters were determined and were found to be $a = b = c = 8.08 \text{ \AA}$. Thermal analysis of the synthesized phosphor suggested weight loss in the form of water and organic molecules, leading to the desired phase formation when annealed at a higher temperature, which was correlated with XRD analysis. The compositional studies determine the presence of Zinc (Zn), Aluminum (Al), Oxygen (O), and Dysprosium (Dy) elements with the appropriate number of atomic percent. FESEM study revealed that the particles have a tendency to aggregate and form small clusters of a typical shape. Using UV–visible Spectroscopy, $\text{ZnAl}_2\text{O}_4:\text{Dy}^{3+}$ phosphor was found to have direct band gap value of 3.91 eV. PL excitation and emission results show that the characteristics 4f–4f transitions of Dy^{3+} ion is responsible for the luminescence properties in the phosphor. The sample which was doped with 0.2 M% doping concentration of dysprosium ion and which was annealed at 1600 °C for 2.0 h showed highest TL intensity. The four hidden peaks were revealed for a typical TL glow curve of $\text{ZnAl}_2\text{O}_4:\text{Dy}^{3+}$ phosphor at 173 °C, 196 °C, 325 °C, and 375 °C. The Computerized Glow Curve Deconvolution (CGCD), Initial Rise (IR) and Variable Heating

Rate (VHR) method were used to find kinetic parameters of TL glow curve and were found to be in decent agreement. All the hidden peaks were discovered to follow first order kinetics. The peak present at lower temperature showed high fading (around 45% fading). However, the peak present at higher temperature showed less fading. The phosphor showed excellent reusability as well as sub-linear and wide dose response in the range 10.0 Gy to 2.0 kGy. Thus, it was found to be a better candidate for the fulfillment of high-dose dosimetry applications.

Acknowledgements NTM gratefully acknowledges Inter-University Accelerator Centre (IUAC), New Delhi for providing funds under the BTR-3 research project code No. UFR-74333. P D Sahare (PDS) is grateful to IoE, University of Delhi, Faculty Research Program, File Ref. No./IoE/2023-24/12/FRP for funding. We are grateful to the Inter university accelerator center (IUAC), New Delhi, for providing the facility of gamma ray ^{60}Co source. Author (PRP) is grateful to the government of India for funding DST-INSPIRE fellowship. Lucky Sharma (LS) wish to gratefully acknowledge a research fellowship by University of Delhi (File No. 7955). One of the authors, (PMK) is very thankful to Chhatrapati Shahu Maharaj Research Training and Human Development Institute (SARTH), Pune, India, for awarding Chhatrapati Shahu Maharaj National Research Fellowship (CSM-NRF)–2020 and providing financial assistance. ARK is thankful to Mahatma Jyotiba Phule Research and Training Institute (Mahajyoti), Nagpur, India, for research fellowship (MJPRF–2021). We thank Miss Preeti Kulkarni for her valuable guidance to handle the TL reader.

Author Contributions Ajay D. Vartha executed most of the experimental work and prepared initial draft of the manuscript, Pratik R. Patankar (PRP) helped in carrying out the experimental work. P. D. Sahare (PDS) arranged funding, facilitated the experimental facilities for irradiation and luminescence work, edited and revised the manuscript, prepared detailed reply to the comments of the respected reviewers, Lucky Sharma (LS) analyzed the XRD data and identified different phases in the materials, Bhuli Bai (BB) helped in recording TL glow curves, Avinash R. Kachere (ARK) helped in literature survey and drafting the manuscript, Prashant M. Kakade (PMK) helped in determination of trapping parameters, Sanjay D. Dhole (SDD) was responsible for overall monitoring and progress of the work, Nandkumar T. Mandlik (NTM) conceived the whole idea and also monitored the progress of the work.

Funding Nandkumar Mandlik: Inter University Accelerator Centre (IUAC), New Delhi, UFR-74333. P D Sahare: IoE, University of Delhi, Faculty Research Program (FRP), File Ref. No./IoE/2023–24/12/FRP. PR Patankar: DST, INSPIRE Fellowship, File No. DST/INSPIRE Fellowship/[IF220184]. Lucky Sharma: University of Delhi, Non-NET Fellowship, File No. 7955. P M Kakade: CSMNRF-2020, File No.CSMNRF-2020/2021–22/109. A R Kachere: MJPRF – 2021, File No. MAHAJYOTI/Nag./Fellowship/2021–22/1042(191).

Declarations

Conflict of interest The authors declare that they have no known competing financial interests or personal relationships that could have appeared to influence the work reported in this paper.

References

- Verma A, Verma A, Bramhe GV (2019) Shifting and enhanced photoluminescence performance of the $\text{Sr}_{1-x}\text{Eu}_x\text{MgAl}_{10}\text{O}_{17}$ phosphor. *J Alloys Compd* 774:1168–1180. <https://doi.org/10.1016/j.jallcom.2018.09.166>
- Mandlik N, Dhole SD, Sahare PD et al (2019) Thermoluminescence studies of CaSO_4 : Dy nanophosphor for application in high dose measurements. *Appl Radiat Isot* 148:253–261. <https://doi.org/10.1016/j.apradiso.2019.03.015>
- Noh AM, Amin YM, Mahat RH, Bradley DA (2001) Investigation of some commercial TLD chips/discs as UV dosimeters. *Radiat Phys Chem* 61:497–499. [https://doi.org/10.1016/S0969-806X\(01\)00313-9](https://doi.org/10.1016/S0969-806X(01)00313-9)
- Madhusoodanan U, Jose M, Tomita A et al (1999) A new thermoluminescence phosphor based on CaSO_4 : Ag, Tm for applications in radiation dosimetry. *J Lumin* 82:221–232. [https://doi.org/10.1016/S0022-2313\(99\)00044-7](https://doi.org/10.1016/S0022-2313(99)00044-7)
- Lakshmanan AR, Jose MT, Ponnusamy V, Kumar PRV (2002) Luminescence in CaSO_4 : Dy phosphor—dependence on grain agglomeration, sintering temperature, sieving and washing. *J Phys D Appl Phys* 35:386–396. <https://doi.org/10.1088/0022-3727/35/4/315>
- Saran M, Sahare PD, Chauhan V, Kumar R, Mandlik NT (2021) Thermoluminescence in Eu doped NaLi_2PO_4 TLD nanophosphor: effect of particle size on TL characteristics. *J Lum* 238:118207
- Kortov VS (2010) Nanophosphors and outlooks for their use in ionizing radiation detection. *Radiat Meas* 45:512–515
- Salah N, Sahare PD, Lochab SP, Kumar P (2006) TL and PL studies on CaSO_4 : Dy nanoparticles. *Radiat Meas* 41:40–47
- Salah N, Sahare PD, Rupasov AA (2007) Thermoluminescence of nanocrystalline LiF:Mg, Cu, P . *J Lumin* 124:357–364
- Lochab SP, Pandey A, Sahare PD, Chauhan RS, Salah N, Ranjan R (2007) Nanocrystalline MgB_4O_7 : Dy for high dose measurement of gamma radiation. *Phys Stat Sol (a)* 204:2416–2425
- Lochab SP, Sahare PD, Chauhan RS, Salah N, Ranjan R, Pandey A (2007) Thermoluminescence and photoluminescence study of nanocrystalline $\text{Ba}_{0.97}\text{Ca}_{0.03}\text{SO}_4$:Eu. *J Phys D: Appl Phys* 40:1343–1350
- Mandlik N, Sahare PD, Kulkarni MS, Bhatt BC, Bhoraskar VN, Dhole SD (2014) Study of TL and optically stimulated luminescence of $\text{K}_2\text{Ca}_2(\text{SO}_4)_3$: Cu nanophosphor for radiation dosimetry. *J Lumin* 146:128–132
- Mandlik N, Sahare PD, Patil BJ, Bhoraskar VN, Dhole SD (2013) Thermoluminescence study of $\text{K}_2\text{Ca}_2(\text{SO}_4)_3$: Cu nanophosphor for gamma ray Dosimetry. *Nucl Instrum Methods Phys Res B* 315:273–277
- Sahare PD, Ranjan R, Salah N, Lochab SP (2007) $\text{K}_3\text{Na}(\text{SO}_4)_2$: Eu nanoparticles for high dose of ionizing radiation. *J Phys D: Appl Phys* 40:759–764
- Mandlik NT, Sahare PD, Rondiya SR, Dzade NY, Deore AV, Dahiwale SS, Dhole SD (2020) Characteristics of $\text{K}_2\text{Ca}_2(\text{SO}_4)_3$: Eu TLD nanophosphor for its applications in electron and gamma rays dosimetry. *Opt Mater* 109:110272
- Mandlik NT, Sahare PD, Dhole SD, Balraj A (2020) Effect of annealing temperature and phase change on thermoluminescence and photoluminescence of $\text{K}_2\text{Ca}_2(\text{SO}_4)_3$: Eu nanophosphor. *Nucl Instrum Methods Phys Res B* 480:105–114. <https://doi.org/10.1016/j.nimb.2020.07.011>
- Mandlik NT, Sahare PD, Kulkarni MS, Rawat NS, Gaikwad NP, Dhole SD (2021) Study of optically stimulated luminescence and calculation of trapping parameters of $\text{K}_2\text{Ca}_2(\text{SO}_4)_3$: Eu nanophosphor. *Appl Radiat Isot* 167:109388
- Mandlik NT, Dhole SD, Sahare PD (2020) Effect of size variation and gamma irradiation on thermoluminescence and photoluminescence characteristics of CaSO_4 : Eu micro and nanophosphor. *Appl Radiat Isot* 159:109080
- Kakade PM, Kachere AR, Sahare PD, Deshmukh AV, Dhole SD, Jadhav SR, Mandlik NT (2022) Structural, compositional and luminescence studies of Y_2O_3 :Eu³⁺ nanophosphor synthesized by sol-gel method. *J Alloys Compd* 928:167106. <https://doi.org/10.1016/j.jallcom.2022.167106>
- Mandlik NT, Varma VB, Kulkarni MS, Bhatt BC, Sahare PD, Raut SA, Mathe VL, Bhoraskar SV, Dhole SD (2020) Luminescence and dosimetric characteristics of nanocrystalline Al_2O_3 : C synthesized by thermal plasma reactor. *Nucl Instrum Methods Phys Res B* 466:90–101
- Mandlik NT, Bhoraskar VN, Patil BJ, Dahiwale SS, Sahare PD, Dhole SD (2017) Thermoluminescence studies of CaSO_4 : Eu nanophosphor for electron dosimetry. *Indian J Pure App Phys* 55:413–419
- Mandlik N, Dhole SD, Sahare PD, Bakare JS, Balraj A, Bhatt BC (2019) Thermoluminescence studies of CaSO_4 : Dy nanophosphor for application in high dose measurements. *Appl Radiat Isot* 148:253–261
- Kulkarni PP, Gavhane KH, Bhadane MS, Bhoraskar VN, Dahiwale SS, Dhole SD (2022) Investigation of thermoluminescence and photoluminescence properties of Tb³⁺, Eu³⁺, and Dy³⁺ doped NaYF_4 phosphors for dosimetric applications. *Phys Chem Chem Phys* 24:11137
- Ali N, Sahare PD, Kachere AR, Kakade PM, Mandlik NT, Dhole SD (2021) Luminescence and dosimetric characteristics of microcrystalline SrB_4O_7 :Eu³⁺ synthesized by solid state diffusion method. *J Radioanal Nucl Chem* 330:1397–1408. <https://doi.org/10.1007/s10967-021-07965-9>
- Bai B, Sahare PD (2023) Effect of redox reactions on the thermoluminescence characteristics of Cu-doped NaLi_2PO_4 phosphors. *RSC adv* 13:20298–20313
- Verma A, Pathak SK, Verma A et al (2018) Tuning of luminescent properties of $\text{Zn}_{1-x}\text{Mg}_x\text{Al}_{10}\text{O}_{17}$: E_u nano phosphor. *J Alloys Compd* 764:1021–1032. <https://doi.org/10.1016/j.jallcom.2018.06.023>
- Meléndrez R, Arellano-Tánori O, Pedroza-Montero M et al (2009) Temperature dependence of persistent luminescence in β -irradiated SrAl_2O_4 :Eu²⁺, Dy³⁺ phosphor. *J Lumin* 129:679–685. <https://doi.org/10.1016/j.jlumin.2009.01.013>
- Toh K, Shikama T, Katsui H et al (2009) Effect of 14-MeV neutrons on strontium–aluminate-based long-lasting phosphor. *J Nucl Mater* 386–388:1027–1029. <https://doi.org/10.1016/j.jnucmat.2008.12.205>
- Kumar RT, Selvam NCS, Ragupathi C et al (2012) Synthesis, characterization and performance of porous Sr(II)-added ZnAl_2O_4 nanomaterials for optical and catalytic applications. *Powder Technol* 224:147–154. <https://doi.org/10.1016/j.powtec.2012.02.044>
- Ciupina V, Carazeanu I, Prodan G (2004) Characterization of ZnAl_2O_4 nanocrystals prepared by coprecipitation and microemulsion techniques. *J Optoelectron Adv Mater* 6:1317–1322
- Van der Laag NJ, Snel MD, Magusin PCMM, de With G (2004) Structural, elastic, thermophysical and dielectric properties of zinc aluminate (ZnAl_2O_4). *J Eur Ceram Soc* 24:2417–2424. <https://doi.org/10.1016/j.jeurceramsoc.2003.06.001>
- Tsai M-T, Chen Y-X, Tsai P-J, Wang Y-K (2010) Photoluminescence of manganese-doped ZnAl_2O_4 nanophosphors. *Thin Solid Films* 518:e9–e11. <https://doi.org/10.1016/j.tsf.2010.03.130>
- Tsai M-T, Chang Y-S, Huang I-B, Pan B-Y (2013) Luminescent and structural properties of manganese-doped zinc aluminate spinel nanocrystals. *Ceram Int* 39:3691–3697. <https://doi.org/10.1016/j.ceramint.2012.10.201>
- Kumari P, Dwivedi Y (2016) Structural and photophysical investigations of bright yellow emitting Dy: ZnAl_2O_4 nanophosphor.

- J Lumin 178:407–413. <https://doi.org/10.1016/j.jlumin.2016.06.027>
35. Mekprasart W, Worasawat S, Tangcharoen T, Pecharapa W (2015) Characterization and effect of calcination temperature on structural properties of spinel zinc aluminate synthesized via Co-precipitation process. *Phys status solidi c* 12:624–627. <https://doi.org/10.1002/pssc.201400292>
 36. Ayvacikli M, Ege A, Yerci S, Can N (2011) Synthesis and optical properties of Er^{3+} and Eu^{3+} doped SrAl_2O_4 phosphor ceramic. *J Lum* 131:2432–2439
 37. Tran MT, Trung DQ, Tu N, Anh DD, Thu LTH, Du NV, Quang NV, Huyen NT, Kien NDT, Viet DX, Hung ND, Huy PT (2021) Single-phase red-emitting $\text{ZnAl}_2\text{O}_4:\text{Cr}^{3+}$ phosphor for application in plant growth LEDs. *J Alloys Compd*. 884:161077
 38. Peng M, Hong G (2007) Reduction from Eu^{3+} to Eu^{2+} in BaAl_2O_4 : Eu phosphor prepared in an oxidizing atmosphere and luminescent properties of BaAl_2O_4 : Eu. *J Lum* 127:735–740
 39. Tai Y, Zheng G, Wang H, Bai J (2015) Broadband down-conversion based near infrared quantum cutting in Eu^{2+} - Yb^{3+} co-doped SrAl_2O_4 for crystalline silicon solar cells. *J Solid State Chem* 226:250–2541. <https://doi.org/10.1016/j.jssc.2015.02.020>
 40. De Camargo ASS, Nunes LAO, Silva JF, Costa ACFM, Barros BS, Silva JEC, De Sá GF, Alves S Jr (2007) Efficient green and red upconversion emissions in $\text{Er}^{3+}/\text{Yb}^{3+}$ co-doped ZnAl_2O_4 phosphor obtained by combustion reaction. *J Phys Condens Mater*. 19:246209. <https://doi.org/10.1088/0953-8984/19/24/246209>
 41. Choudhary AK, Singh SK, Dwivedi A, Bahadur A, Rai SB (2018) Enhanced upconversion emission of $\text{Er}^{3+}/\text{Yb}^{3+}$ and $\text{Er}^{3+}/\text{Yb}^{3+}/\text{Zn}^{2+}$ doped calcium aluminate for use in optical thermometry and laser induced optical heating Method. *Appl Fluoresc* 6:035014. <https://doi.org/10.1088/2050-6120/aac8f9>
 42. Sharma L, Sahare PD (2023) Mechanoluminescence, thermoluminescence, optically stimulated luminescence and photoluminescence in SrAl_2O_4 : Eu micro- and nanophosphors: effect of particle size and annealing in different atmospheres. *RSC Adv* 13:25579. <https://doi.org/10.1039/d3ra02514d>
 43. Salah N, Sahare PD, Nawaza S, Lochab SP (2004) Luminescence characteristics of $\text{K}_2\text{Ca}_2(\text{SO}_4)_3$:Eu, Tb micro- and nanocrystalline phosphor. *Radiat. Eff Defects Solids* 159:321–334
 44. Pandey A, Sharma VK, Mohan D, Kale RK, Sahare PD (2002) Thermoluminescence characteristics of $\text{K}_2\text{Ca}_2(\text{SO}_4)_3$ doped with rare earths Eu and Dy. *J Phys D: Appl Phys* 35:1330–1333
 45. Pandey A, Sahare PD (2003) Thermoluminescence characteristics of LiNaSO_4 doped with rare earths Eu and Dy. *Phys Stat Sol (a)* 199:533–540. <https://doi.org/10.1002/pssa.200306655>
 46. Rani G, Sahare PD (2013) Effect of temperature on structural and optical properties of Boehmite nanostructure. *Int J Appl Ceram Technol* 12:124–132. <https://doi.org/10.1111/ijac.12133>
 47. Kumari S, Sahare PD (2013) Optical studies of fluorescent mesoporous silica nanoparticles. *J Mater Sci Technol* 29:742–746. <https://doi.org/10.1016/j.jmst.2013.05.013>
 48. Wu X, Wei Z, Chen X et al (2017) Effects of cobalt doping on the microstructure and optical properties of ZnAl_2O_4 nanoparticles. *Russ J Phys Chem A* 91:2651–2656
 49. Satapathy KK, Mishra GC, Khan F (2015) ZnAl_2O_4 : Eu novel phosphor: SEM and mechanoluminescence characterization synthesized by solution combustion technique. *Luminescence* 30:564–567. <https://doi.org/10.1002/bio.2786>
 50. Habibi MK, Rafiaei SM, Alhaji A, Zare M (2021) ZnAl_2O_4 : Ce^{3+} phosphors: study of crystal structure microstructure, photoluminescence properties and efficient adsorption of Congo red dye. *J Molec Struct* 1228:129769
 51. Juibari NM, Eslami A (2016) Investigation of catalytic activity of ZnAl_2O_4 and ZnMn_2O_4 nanoparticles in the thermal decomposition of ammonium perchlorate: structural and kinetic studies. *J Therm Anal Calorim*. <https://doi.org/10.1007/s10973-016-5906-8>
 52. Gama L, Ribeiro MA, Barros BS et al (2009) Synthesis and characterization of the NiAl_2O_4 , CoAl_2O_4 and ZnAl_2O_4 spinels by the polymeric precursors method. *J Alloys Compd* 483:453–455. <https://doi.org/10.1016/j.jallcom.2008.08.111>
 53. Sampath SK, Kanhere DG, Pandey R (1999) Electronic structure of spinel oxides: zinc aluminate and zinc gallate. *J Phys Condens Matter* 11:3635–3644. <https://doi.org/10.1088/0953-8984/11/18/301>
 54. Pouran M, Farzad D, Mahsa M (2019) Ternary $\text{ZnO}/\text{ZnAl}_2\text{O}_4/\text{Al}_2\text{O}_3$ composite nanofiber as photocatalyst for conversion of CO_2 and CH_4 . *Ceram Int*. <https://doi.org/10.1016/j.ceramint.2019.09.009>
 55. Jagadeeshwaran C, Murugaraj R (2019) Impact of sintering temperature on the structural, optical, and electrical properties of zinc aluminate. *J Mater Sci: Mater Electr*. <https://doi.org/10.1007/s10854-019-01951-4>
 56. Wachter W, Vana NJ, Aiginger H (1980) The influence of hydroxyl ions on the thermoluminescence properties of $\text{LiF}:\text{Mg, Ti}$. *Nucl Instr Methods* 175:21–23
 57. Stoebe TG, DeWerd LA (1985) Role of hydroxide impurities in the thermoluminescent behavior of lithium fluoride. *J Appl Phys* 57:2217–2220. <https://doi.org/10.1063/1.334365>
 58. Rani G, Sahare PD (2013) Effect of phase transitions on thermoluminescence characteristics of nanocrystalline alumina. *Nucl Instr Meth Phys Res B* 311:71–77. <https://doi.org/10.1016/j.nimb.2013.06.018>
 59. Sahare PD, Bakare JS, Dhole SD, Kumar P (2012) Effect of phase transition and particle size on thermoluminescence characteristics of nanocrystalline $\text{K}_2\text{Ca}_2(\text{SO}_4)_3$: Cu^+ phosphor. *Radiat Measur* 47:1083–1091
 60. Rani G, Sahare PD (2014) Study of the structural and morphological changes during the phase transition of ZnS to ZnO . *Appl. Phys A* 116:831–837
 61. Bos AJJ (2006) Theory of thermoluminescence. *Radiat Meas* 41:S45–S56. <https://doi.org/10.1016/j.radmeas.2007.01.003>
 62. Kalita JM, Chithambo ML (2017) Thermoluminescence of $\alpha\text{-Al}_2\text{O}_3$:C, Mg: Kinetic analysis of the main glow peak. *J Lumin* 182:177–182. <https://doi.org/10.1016/j.jlumin.2016.10.031>
 63. Rasheedy MS, Amry AMA (1995) Luminescence on the frequency factor obtained in case of thermoluminescence second order kinetics. *J Lumin* 63:149–154
 64. Kitis G, Gomez-Ros JM, Tuyn JWN (1998) Thermoluminescence glow-curve deconvolution functions for first, second and general orders of kinetics. *J Phys D Appl Phys* 31:2636–2641. <https://doi.org/10.1088/0022-3727/31/19/037>
 65. Pagonis V, Kitis G, Furetta C (2006) Numerical and practical exercises in thermoluminescence, Springer New York, NY. ISBN: 978-0-387-26063-1. <https://doi.org/10.1007/0-387-30090-2>
 66. Chen R, Kirsh Y (1981) Analysis of thermally stimulated processes. Pergamon Press, New York, USA
 67. Balarin M (1979) Temperature Dependence of the Pre-Exponential Factor in the Glow Curve Theory *J Therm Anal* 17:319. <https://doi.org/10.1002/pssa.2210540257>
 68. Chen R, Huntley DJ, Berge GW (1983) Analysis of Thermoluminescence Data Dominated by Second-Order Kinetics *phys stat sol (a)* 79:251. <https://doi.org/10.1002/pssa.2210790128>
 69. Garlick GFJ, Gibson AF (1948) The Electron Trap Mechanism of Luminescence in Sulphide and Silicate Phosphors. *Proc Phys Soc* 60:574
 70. May CE, Partridge JA (1964) Thermoluminescent kinetics of alpha-irradiated alkali halides. *J Chem Phys* 40:1401–1409. <https://doi.org/10.1063/1.1725324>
 71. Rasheedy MS (1993) On the general-order kinetics of the thermoluminescence glow peak. *J Phys: Condens Matter* 5:633. <https://doi.org/10.1088/0953-8984/5/5/014>

72. Nucleonix Systems PVT LIMITED India, (2023). <https://www.nucleonix.com>

Publisher's Note Springer Nature remains neutral with regard to jurisdictional claims in published maps and institutional affiliations.

Springer Nature or its licensor (e.g. a society or other partner) holds exclusive rights to this article under a publishing agreement with the author(s) or other rightsholder(s); author self-archiving of the accepted manuscript version of this article is solely governed by the terms of such publishing agreement and applicable law.